Research Article

Potent pharmacophoric aminothiazole derivatives as FabH inhibitors for antibacterial activity: in vitro and in silico approach

Nadine Uwabagira[1] · Balladka K. Sarojini[1,2] · Madan K. Shankar[3] · Ramesh S. Gani[2]

Abstract
The present work reports the design, synthesis, characterization and antibacterial screening of novel aminothiazole derivatives as FabH inhibitor [*β*-ketoacyl-ACP synthase (KAS)] which plays major role in bacterial cell wall construction. The compound **5d** had crystallized in monoclinic, *P21/c* space group which was determined by single-crystal X-ray crystallography. In vitro antibacterial activity studies were carried out on *S. aureus* (MCC 2043), *E. faecalis* (MTCC 2729), *E. coli* MTCC443 and *C. violaceus* (MCC 2216). Most of the compounds showed potent inhibition activity against Gram-negative bacteria than Gram-positive bacteria. Compound **5a** showed the highest zone of inhibition of 16 mm and MIC value of 5.33 µM which is comparable to that of the standard antibiotic, streptomycin. This result was ably complimented by in silico studies where compound **5a** exhibited high affinity, strong binding energy and docking score of 6.214 kcal mol^{-1}. The most potent compounds were nonhemolytic and nontoxic to mammalian cells.

Keywords Aminothiazole · Single crystal · The β-ketoacyl-ACP synthase (KAS) I · Antibacterial activity · Molecular docking · Molecular dynamic simulations

1 Introduction

Bacterial infections cause dangerous diseases and in many nations, a great number of mortality is seen especially in developing countries. These infectious diseases spread quickly and affect mostly the immunocompromised people, pregnant women, children, and older individuals [1]. Bacterial survival mostly depends on fatty acid biosynthesis. Three pathways are required for initiation of fatty acid biosynthesis; firstly β-ketoacyl-ACP synthase (KAS) III helps the condensation of acetyl-CoA and malonyl-CoA, secondly, there is a transfer of acetate moiety from acetyl-CoA to acetyl-ACP either by acetyl-CoA:ACP transacylase or β-ketoacyl-ACP synthase (KAS) III. Thirdly, there is a decarboxylation of malonyl-ACP by synthase I to form acetyl-ACP which will be condensed with malonyl-ACP by synthase I [2]. The β-ketoacyl-ACP synthase (KAS) I is the only condensing enzyme required for the initiation of fatty acid biosynthesis [3]. Initially, this protein was inhibited by antibiotics such as thiolactomycin and cerulenin in bacteria and plants but in *Saccharomyces cerevisiae* and mammals there is appearance of antibiotic resistance [4]. In contrast, cerulenin specifically inhibits condensing enzyme which is β-ketoacyl thioester synthetase whereas thiolactomycin is able to inhibit the type II fatty acid synthetase [5] but inactive to type I. Extensive studies confirmed that excessive production of β-ketoacyl-ACP synthase (KAS) I contribute to thiolactomycin resistance to *E. coli* [6]. As some antibiotics have limitation of developing resistance

Electronic supplementary material The online version of this article (https://doi.org/10.1007/s42452-019-1298-2) contains supplementary material, which is available to authorized users.

✉ Balladka K. Sarojini, bksaroj35@gmail.com | [1]Biochemistry Division, Department of Chemistry, Mangalore University, Mangalagangothri, Karnataka 574199, India. [2]Department of Industrial Chemistry, Mangalore University, Mangalagangothri, Karnataka 574199, India. [3]PURSE Lab, Mangalore University, Mangalagangothri, Karnataka 574199, India.

SN Applied Sciences (2019) 1:1375 | https://doi.org/10.1007/s42452-019-1298-2

Received: 17 May 2019 / Accepted: 17 September 2019 / Published online: 11 October 2019

or losing their potency, further research in this direction can be undertaken for optimal drug development.

Thiazole and its derivatives are known as active pharmaceutical ingredients in several drugs for their potential as anti-inflammatory [7, 8] anti-HIV, antiproliferative [9, 10], antibacterial and antifungal activity [11, 12]. Furthermore, extensive research has been carried out on thiazole scaffolds for their anticancer [13] antimicrobial [14], antiallergy [15] and as central dopamine agonist agents [16]. The most prominent role played by thiazole compounds in general is found to be against multi-drug resistant tumor [17] and in the treatment of type-2 diabetes [18].

There are many factors for bacteria to survive; among those factors fatty acid biosynthesis is essential as it is required for cell viability and growth [19]. Initiating fatty acid elongation cycles [20, 21] and involving in the feedback regulation of the biosynthetic pathway via product inhibition [22], make it a promising target for the design of novel antibacterial drugs.

In view of the above mentioned findings, in the present work, we report the design, synthesis, characterization and antibacterial activity of new series of aminothiazole derivatives against *E. coli* fatty acid biosynthesis (FabH). In vitro antibacterial activities were carried out on *S. aureus* (MCC 2043), *E. faecalis* (MTCC 2729), *C. violaceus* (MCC 2216) and *E. coli* (MTCC443). In addition, docking simulations were performed to position all synthesized compounds into the *E. coli* FabH active site to determine the probable binding conformation. The ten novel synthesized compounds were well characterized by ^{1}H NMR, ^{13}C NMR, FTIR, LCMS data and elemental analysis. The results of such studies are presented in this paper.

2 Results and discussion

2.1 Chemistry

The synthesis of new series of compounds is outlined in Scheme 1. The key intermediate, substituted phenylthiourea **2** was obtained from the reaction of ammonium thiocyanate on substituted aniline derivative **1** in concentrated HCl under reflux condition [23]. The substituted 4-phenacylbromides **4** were prepared by bromination of respective acetophenones **3** in chloroform solvent [24]. The new series of substituted phenyl thiazol-2-amine **5a**–**j** was synthesized by refluxing a mixture of substituted phenylthiourea derivatives **2** and 4-substituted phenacylbromides **4** in ethanol in the absence of any catalyst. The formation of the title compounds **5a**–**j** was confirmed by their analytical and spectral data.

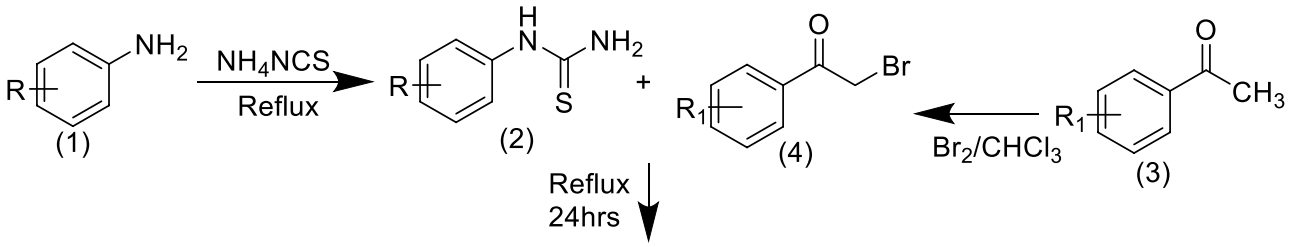

R	R_1
5a=3,4-Cl	**5a**=4-NO_2
5b=4-NO_2	**5b**= 4-F
5c=3,4-Cl	**5c**=4-Cl
5d=2,6-CH_3	**5d**=4-Cl
5e=2-CH_3-3-Cl	**5e**=4-NO_2
5f= 2-CH_3-3-Cl	**5f**=4-Cl
5g=2-CH_3-3-Cl	**5g**=4-OCH_3
5h=2-CH_3-4-F	**5h**=4-Cl
5i= 2,6-CH_3	**5i**=4-Cl
5j=2,6-CH_3	**5j**=4-NO_2

Scheme 1 Synthesis of the title compounds (**5a**–**j**)

The spectral details of representative compound **5a** are as follows: in the IR spectrum of **5a**, an absorption band found at 3126 cm^{-1} was attributed to NH stretch. The absorption bands seen at 1494 cm^{-1} and 1616 cm^{-1} were due to the stretching frequency of –C=N– and –C=C– respectively. The presence of nitro group in the product was evidenced by two prominent absorption bands appearing at 1552 cm^{-1} and 1319 cm^{-1} for the antisymmetric and symmetric stretching frequencies of NO_2 group. Likewise, an absorption band appeared at 725 cm^{-1} proved the presence of –C–Cl stretching. On recording ^{1}H NMR spectrum, the formation of thiazole amine derivative **5a** was supported by the presence of respective signals for the protons present in the molecule. A singlet seen at δ (ppm) 7.44 could be accounted for the thiazole ring proton. The two sets of ortho and meta protons of 4-nitro phenyl ring were seen as doublets centered at 8.25 (J = 8 Hz) and 8.12 (J = 8 Hz) respectively. A doublet appeared at δ (ppm) 7.66 (J = 2.6 Hz) and 7.62 (J = 2.7 Hz) was accounted for one of ortho and meta protons of 3,4-dichlorophenyl ring respectively, and two singlets found at δ (ppm) 7.47 and δ (ppm) 8.17 were assigned to another ortho proton of 3,4-dichlorophenyl ring and thiazole proton respectively. The exocyclic NH proton appeared at δ (ppm) 10.58 as a singlet. This data confirmed the formation of the title compound **5a**.

Furthermore, it was supported by recording ^{13}C NMR spectrum. The signals appeared in the spectrum could be assigned to the exact number of carbon atoms including magnetically equivalent ones. Molecular mass of **5a** was determined by LCMS and was found to be 366.00 $(M+H)^+$.

Similarly, the structure of all the synthesized molecules was determined by spectroscopic characterization and is given in experimental section.

2.2 Single crystal X-ray crystallography of the compound 5d

In order to determine the three dimensional structure of the title compounds, they were subjected to crystal growth by slow evaporation technique in suitable solvent. However, only the compound **5d** was crystallized in a defractable form and the details of the crystal structure and data refinement are given in Table 1.

Molecular structure of the compound **5d**, showing the atomic numbering system. Displacement ellipsoids are drawn at the 50% probability. Dotted lines indicate intermolecular hydrogen bonds. The **5d** molecule crystallized in monoclinic crystal system (space group *P21/c*) with unit cell parameters a = 14.0755(10), b = 8.5068(3), c = 15.4086(10), β = 108.390(7), volume = 1750.77(19) $Å^3$ and Z = 4. The ORTEP of **5d** is shown in Fig. 1. The

Table 1 Crystal data and structure refinement details for compound **5d**

CCDC	1845758
Empirical formula	$C_{17}H_{16}N_2ClSBr$
Formula weight	395.74
Temperature (K)	293(2)
Wavelength (Kα, Å)	0.71075
Crystal system, space group	monoclinic, *P21/c*
Unit cell dimensions (Å, °)	*a* = 14.0755(10) *b* = 8.5068(3) *c* = 15.4086(10) β = 108.390(7)
Volume $Å^3$	1750.77(19)
Z, Calculated density (Mg m^{-3})	4 1.501
Absorption coefficient (mm^{-1})	2.617
$F_{(000)}$	800
Crystal size (mm)	0.210 × 0.230 × 0.25
Theta range for data collection (°)	2.7 to 50.0
Limiting indices	$-16 \le h \le 16, -10 \le k \le 10, -18 \le l \le 18$
Reflections collected/unique[R(int)]	17,243/3087 [0.042]
Refinement method	Full-matrix least-squares on F^2
Data/restraints/parameters	2592/0/201
R value	0.0323
Goodness-of-fit on F^2	1.02
Largest diff. peak and hole (e. $Å^{-3}$)	0.30 and –0.26

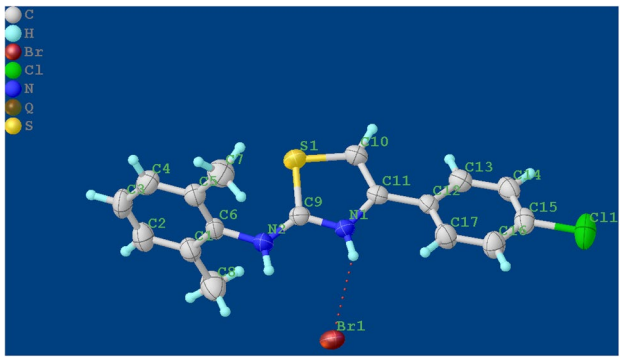

Fig. 1 The ORTEP of compound **5d**

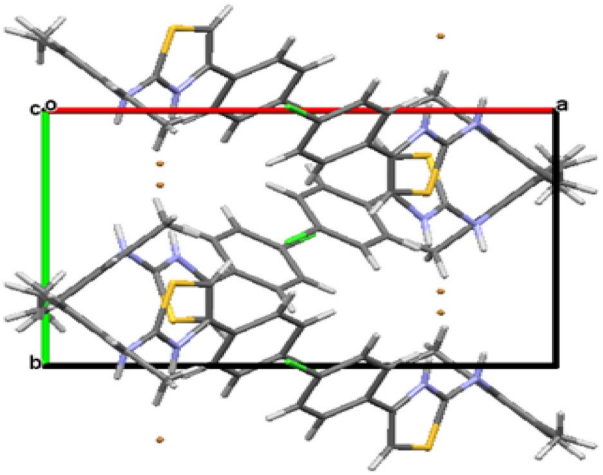

Fig. 2 Packing of the compounds: a view along *c*-axis

thiazole ring (Cg1: S1/C9/N1/C11/C10) makes a dihedral angle of 72.65(14)° and 25.47(14)° with methyl phenyl ring (Cg2:C1–C6) and chlorophenyl ring (Cg3:C12–C17), respectively. The dihedral angle between Cg2 and Cg3 is 82.24(14)°. Intramolecular hydrogen bonds N1–H1…Br1 and N2–H2…Br2 were observed. As one of the products in condensation was HBr (Scheme 1), the nitrogen of thiazole ring in compound **5d**, got protonated converting to quaternary nitrogen and the Br^- existed as counter ion which is evident from Fig. 1.

In the crystal structure (Table 2 and Fig. 2), the molecules are stabilized through intermolecular interactions of the type C15–Cl1…Cg1, Cg2…Cg2 (3.77(17) Å, slippage 1.301, symmetry = −x, 1−y, −z) and Cg3…Cg3 [(3.72(17) Å, slippage 1.283, symmetry = 1−x, 1−y, 1−z).

3 Biological evaluations

3.1 Antibacterial studies

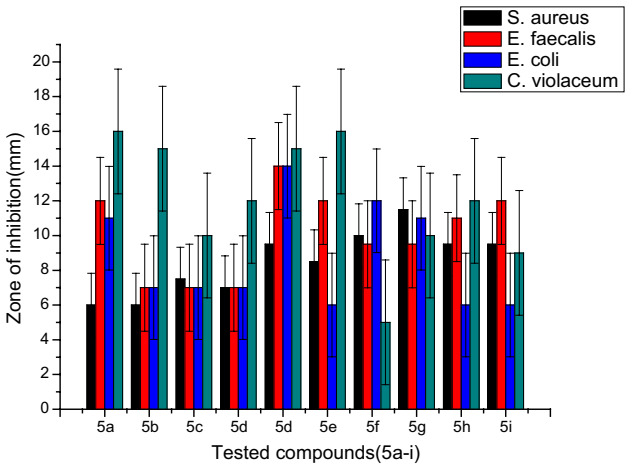

Fig. 3 Antibacterial activity by zone of inhibition (mm)

All the tested compounds exhibited moderate activity against the four strains taken for evaluation (Fig. 3). Among tested compounds **5a**, **5b**, **5c**, **5d**, **5e** and **5i** have inhibited *E. coli* (MTCC443) effectively than other bacterial strains. The compounds **5a**, **5e**, **5f** and **5i** were found to be active against *C. violaceum* (MCC 2216) whereas **5a**, **5e**, **5g** and **5h** were effective against *E. faecalis* (MTCC 2729). The nitro and halo substitutions on either side of the phenyl rings affected the bactericidal property of the tested thiazole derivatives. But none of the title compounds were potent enough to arrest the growth of *S. aureus* (MCC 2043).

The compounds which exhibited notable zone of inhibition for the microbes were taken for the determination of MIC along with the standard streptomycin (Fig. 4). Among the active ones, the compound **5a** emerged as most potent one against all the tested strains with MIC of 5.33 µM which is comparable to standard drug (streptomycin).

Table 2 Intermolecular and intramolecular interactions

D–H/X…A/Cg	D–H/X Å	H/X…A/Cg Å	D…A/Cg Å	D–H/X…A/Cg (°)	Symmetry/centroid
N1–H1…Br1	0.86	2.45	3.1765(17)	143	
N2–H2…Br2	0.86	2.67	3.3619(18)	139	
C15–Cl1…Cg1^{i}		3.6232(15)	4.100(3)	92.95(11)	1−X, 1−Y, 1−Z

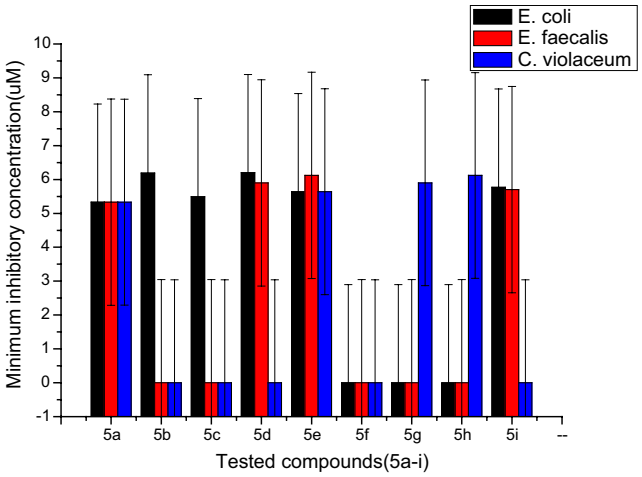

Fig. 4 Minimal inhibition concentration (MIC) in μM

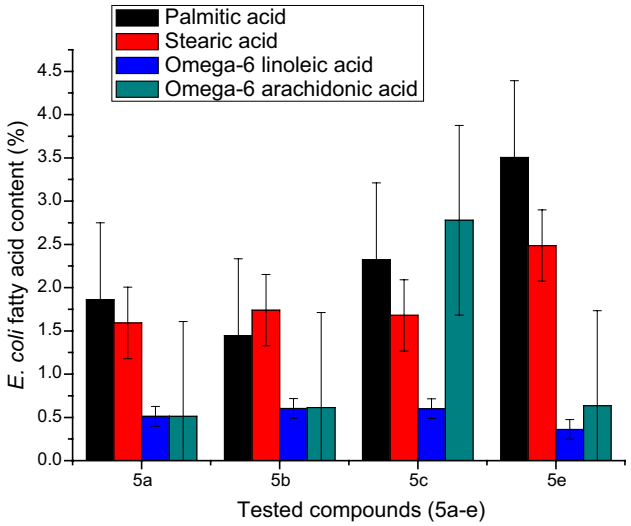

Fig. 5 *E. coli* fatty acid content (%)

3.2 Fatty acids inhibition activity

In the positive standard which is *E. coli* MTCC443, assays were conducted to estimate different fatty acids levels and after the study, the fatty acid levels were found to be considerably low in the tested samples incubated along with *E. coli*. For saturated fatty acids, palmitic and stearic acids percentage for **5a**, **5b**, **5c** and **5e** were (1.862, 1.592); (1.446, 1.740); (2.322, 1.679) and (3.504, 2.486) respectively and the control (bacterial culture) was having three times greater the amount of fatty acid and was (3.634, 4.554). For monounsaturated fatty acids, only palmitoleic acid was 1.676, 1.502, 0.891 and 0.377% for **5a**, **5b**, **5c** and **5e** while the positive control was 2.158%.

However, (ω-3) polyunsaturated fatty acids were not detected in the positive control and the samples treated with test compounds as well. Besides, (ω-6) polyunsaturated fatty acids (PUFA) were present and the percentage was almost zero indicating complete inhibition. For ω-6 PUFA (Linoleic acids) percentage of inhibition for **5a**, **5b**, **5c** and **5e** was 0.512, 0.614, 2.779 and 0.635% respectively and 7.121% for the control. The ω-6 PUFA (Arachidonic acids) percentage for **5a**, **5b**, **5c** and **5e** was 0.512, 0.604, 0.601 and 0.361% respectively and 5.251% for the control. The other fatty acids such as oleic, myristoleic, alpha linoleic, eicosapentaenoic, docosapentaenoic, docosahexaenoic, gamma linoleic and dihomo gamma linoleic acids were not found in the tested samples treated with the test samples. Among the tested compounds, compound **5a** emerged as most potent one. The (Fig. 5) shows the results of *E. coli* fatty acid content after treating with the tested compounds. This result probably shows the ability of the tested compounds in reducing the bacterial (*E. coli*) fatty acid content.

3.3 Hemolysis assay

The tested compounds were effective in inhibiting essential fatty acids in the microbial cell. It is assumed that similar array of fatty acids are also present in the human cells. So the evaluation of toxicity to human cells by the tested compounds was carried out by haemolysis assay. The percentage of haemolysis ranged between 0.88 and 12.27. The human blood toxicity activity of the tested compounds at minimum tested concentration of 12.5 μg mL^{-1} is in ascending order was as follows: **5a** < **5c** < **5b** < **5e** < **5j**. The maximum concentration of 100 μg mL^{-1} could do lysis only up to 12.27% for compound **5j**. The hemolysis assay showed that all tested compounds were less toxic on human blood especially the compound **5a** and **5b**. All the tested compounds were found to possess minimum toxicity towards human blood cells as it was evidenced by the value given in Table 3 and Fig. 6.

The Fig. 6 showed how the tested compounds are less toxic on human blood even at higher concentration (100 μg mL^{-1}), the toxicity is less. Except the compound **5j**, the toxicity of the rest tested compounds is nearly indirectly proportional to the concentration of the sample and could be tolerable (**5b**, **5a**, **5c** and **5e** respectively).

3.4 Molecular docking studies

The *E. coli* FabH (PDB ID: 5BNR) protein was docked into the active site of the model structure of FabH using Schrödinger Software, the ligands were prepared by ligprep, protein was prepared by protein preparation wizards, the Glide was generated by receptor grid generation for bioactive conformation searching then docking was

Table 3 Percentage of hemolysis

Sample code	Sample concentration (μg mL^{-1})	Sample % haemolysis
5a	100	4.59
	50	3.57
	25	3.37
	12.5	**0.88**
5b	100	3.87
	50	3.60
	25	3.40
	12.5	**2.18**
5c	100	8.26
	50	4.76
	25	2.82
	12.5	**2.04**
5e	100	5.81
	50	5.00
	25	3.74
	12.5	**2.19**
5j	100	12.27
	50	10.50
	25	4.04
	12.5	**2.58**

The least concentration and hemolysis % are in bold to show how the compound concentration is directly proportional to the % of hemolytic activity

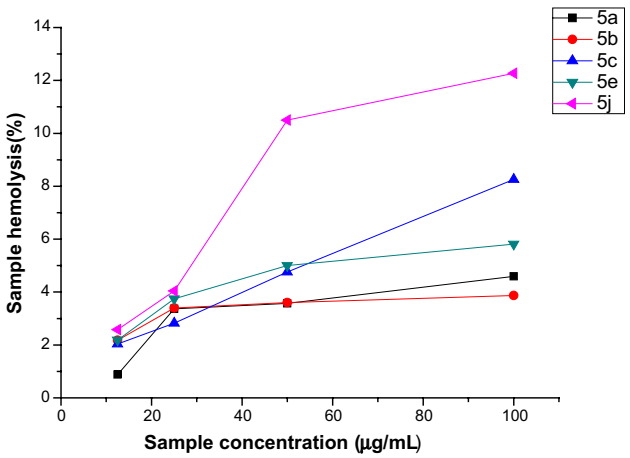

Fig. 6 Hemolysis essay results

done by extra precision (XP). The root mean square deviation (RMSD) was found to be 0.2949 which is reasonable as generally it should be less than 2. The binding models as well as the ligand interaction diagrams of the potent compounds and *E. coli* FabH are depicted in the figures below.

***Interaction of 5a*:** The *E. coli* FabH amino acids formed two strong hydrogen bonds (Asn^{274} with distance between the bond of 2.78 Å, angle of 112.7) and Cys^{112} with distance between the bond of 2.19 Å, angle of 158.2 Å) and two halogen bonds (Asn^{210} with distance of 2.85 Å, angle of 127.3 Å and dihedral of 39.6 Å), (Arg^{36} with distance of 2.52, angle of 127.2 Å, dihedral of 113.3 Å) with the compound **5a** (Fig. 7).

***Interaction of 5b*:** The *E. coli* FabH amino acids formed two strong hydrogen bonds (Asn^{274} with distance of 2.28, angle of 112.4 Å), Cys^{112} with distance of 2.23 Å, angle of 99.3 Å), one π–cation with Arg^{249} with distance of 4.68 Å, angle of 66.4 Å, dihedral of 159.3) and one aromatic hydrogen with Gly^{209} with distance of 2.46 Å, angle of 121.9 Å and dihedral of 49 Å (Fig. 8).

***The interaction of 5c*:** The *E. coli* FabH amino acids formed five bonds: One π–cation with (Met^{1} with distance between the bond of 2.2 Å, angle of 94.2, and dihedral of 53.6), three aromatic hydrogen bonds: (Asp^{123} with distance between the bond of 2.74 Å, angle of 109.7 Å and dihedral of 158.7 Å), Ile^{174} with distance of 2.46 Å, angle of 92.3 Å, dihedral of 121.6 Å) and (Met^{1} with distance of 0.82 Å, angle of 125.3 Å, dihedral of 179.1 Å) and one halogen bonds with Lys^{127} with distance between the bond of 1.63 Å, angle of 143.5 Å and dihedral of 30.4 Å) (Fig. 9).

The interaction of 5e The *E. coli* FabH amino acids formed one strong hydrogen bonds (Ser^{169} with distance between the bonds was 2. 17 Å, angle of 116.3 Å), two aromatic hydrogen bonds with Asp^{123} with distance between the bond was 2.72 Å, angle of 136.1 Å) and (Ile^{175} with distance between the bond of 2.21 Å, angle of 104.5 Å). Two halogen bonds with (Ile^{175} with distance of 3.27 Å, angle of 156.6 Å, dihedral of 24.9 Å) and (Lys^{127} with distance of 2.86 Å, angle of 116.0 Å, dihedral of 40.9 Å) (Fig. 10). The Table 4 showed Bonds, hydrophobic interactions and D-scores of the synthesized compounds.

3.5 Molecular dynamic simulations of the compound 5a

While docking, protein flexibility was not considered, in that occasion, molecular dynamic simulations were done with the Desmond program to confirm the mode of ligand binding as well as the stability of protein–ligand complex. The compound **5a** was showing the promising results and so was taken for molecular dynamic simulations (Figs. 11, 12, 13).

(RMSD) stands for the root mean square deviation and is the measurement of the atoms displaced and the last is directly proportional to the reference time.

The RMSD for frame x is:

$$RMSD_x = \sqrt{\frac{1}{N}\sum_{i=1}^{N}(r_i'(t_x)) - (r_i(t_{ref}))^2}$$

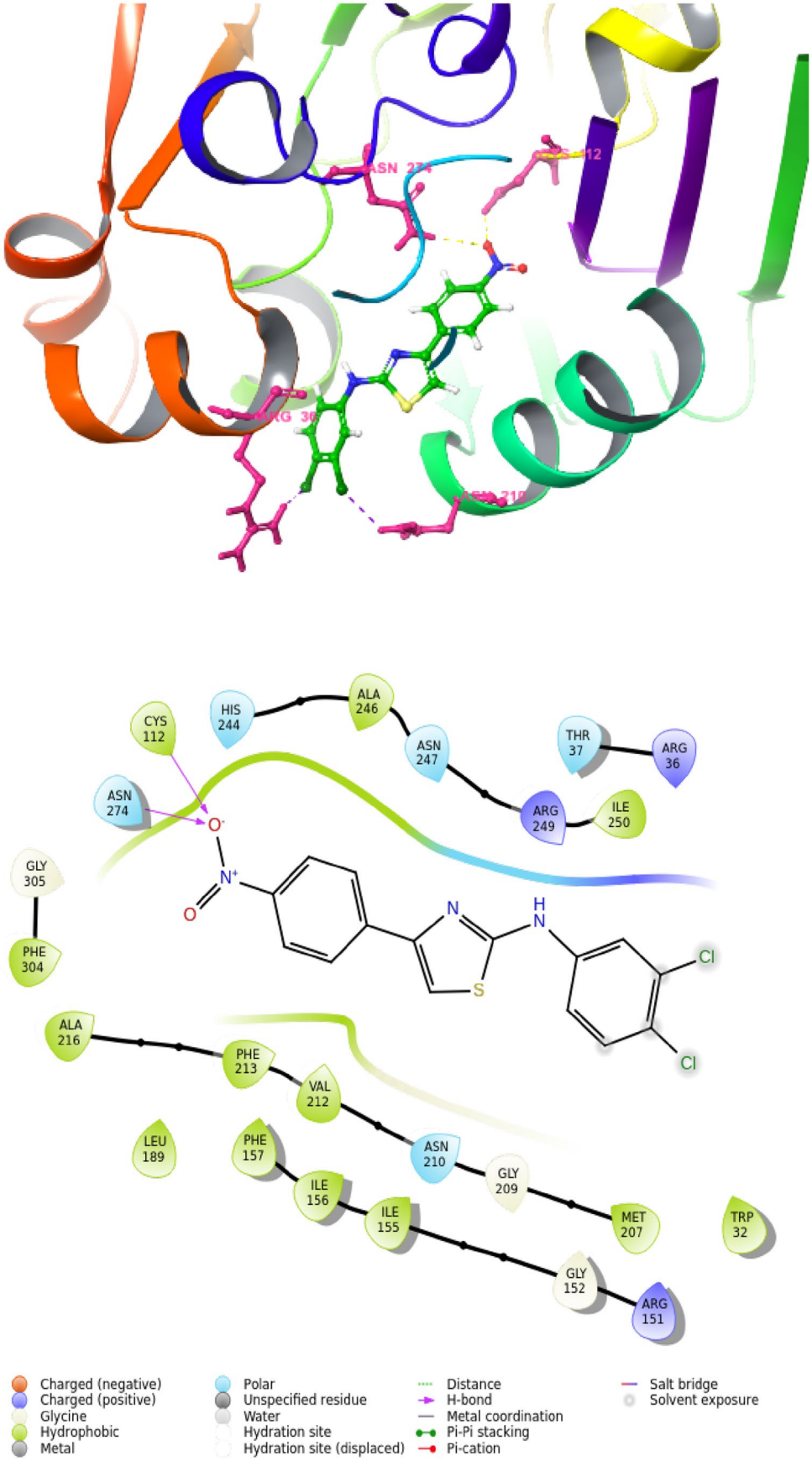

Fig. 7 Docking poses of the compound **5a** with *E. coli* FabH (PDB Id-5BNR)

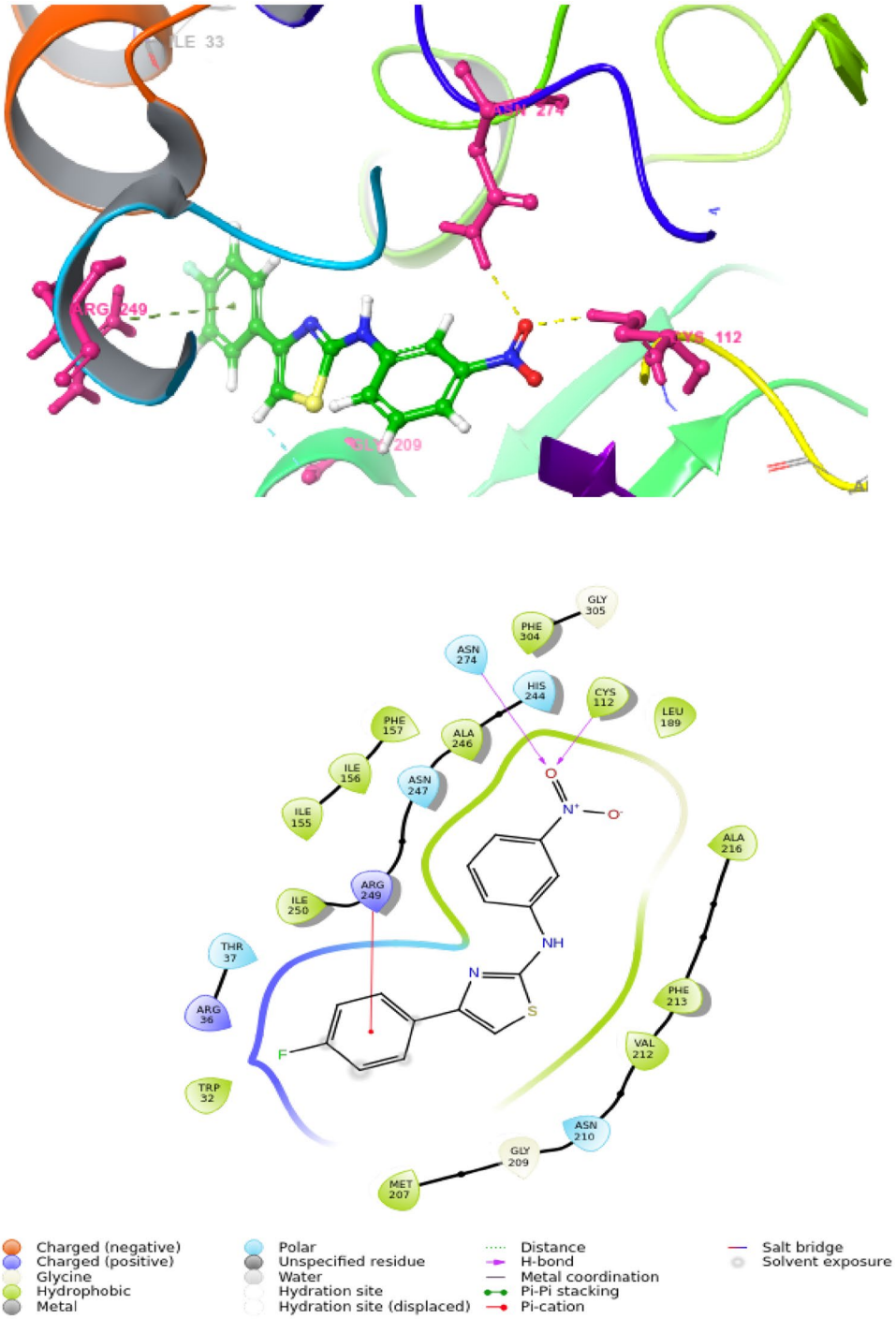

Fig. 8 Docking pose of the compound **5b** with *E. coli* FabH (PDB Id-5BNR)

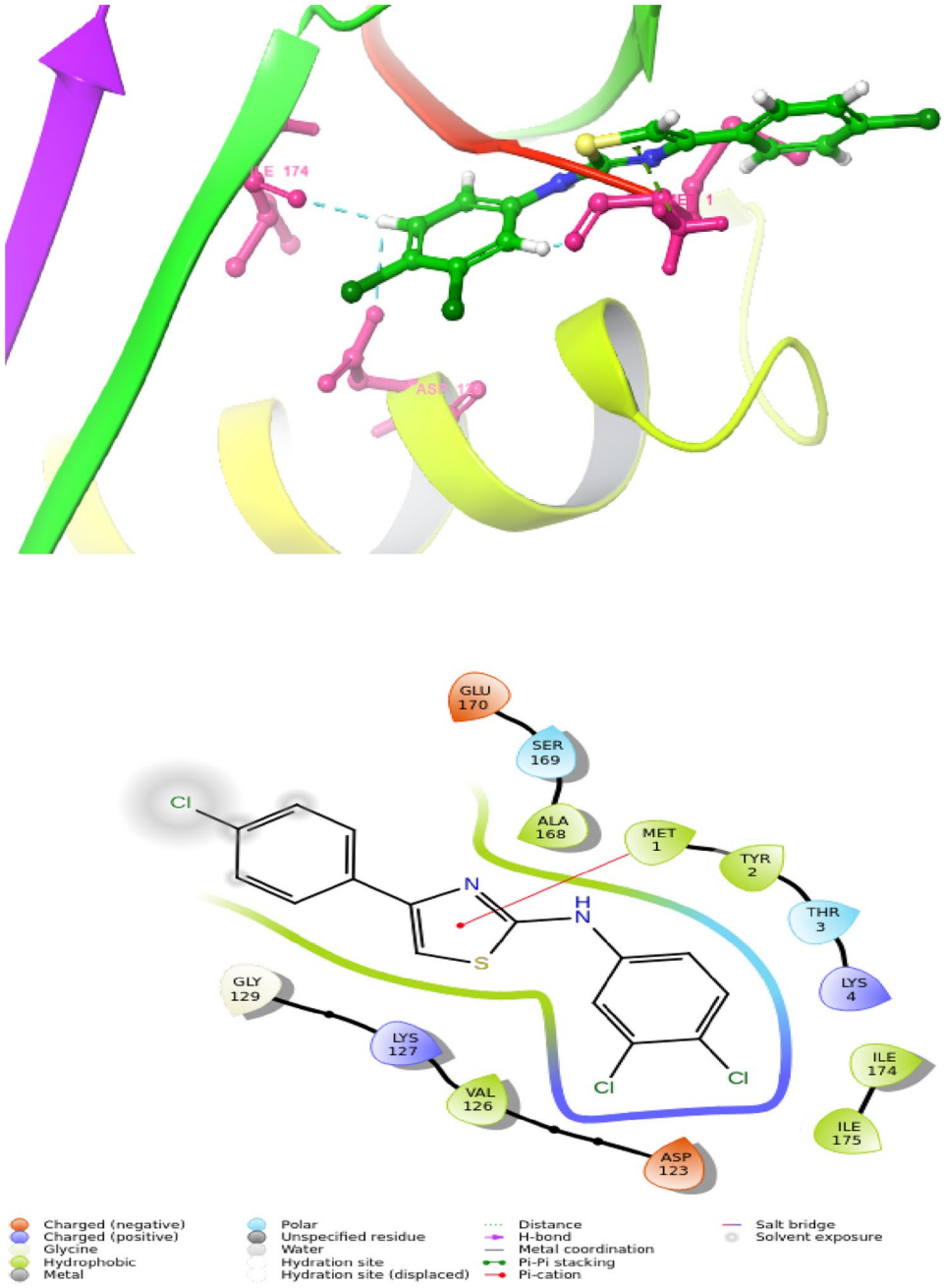

Fig. 9 Docking pose of the compound **5c** with *E. coli* FabH (PDB Id-5BNR)

N, the number of selected atoms; t_{ref}, the reference time (first frame, t = 0); r′ = the position of selected atom in the frame x which is recorded at time t_x.

Protein RMSD found on the left Y-axis, RMSD is calculated on the basis of selected atom and its analysis gives the structural conformation.

Ligand RMSD found on right-Y-axis and showed the ligand stability.

The root mean square fluctuation (RMSF) characterizing local change with the protein chain showing the flexibility of each residue.

The RMSF for residue *i* is:

$$RMSF_i = \sqrt{\frac{1}{T}\sum_{t=1}^{T}\left\langle (r_i'(t)) - (r_i(t_{ref}))^2 \right\rangle}$$

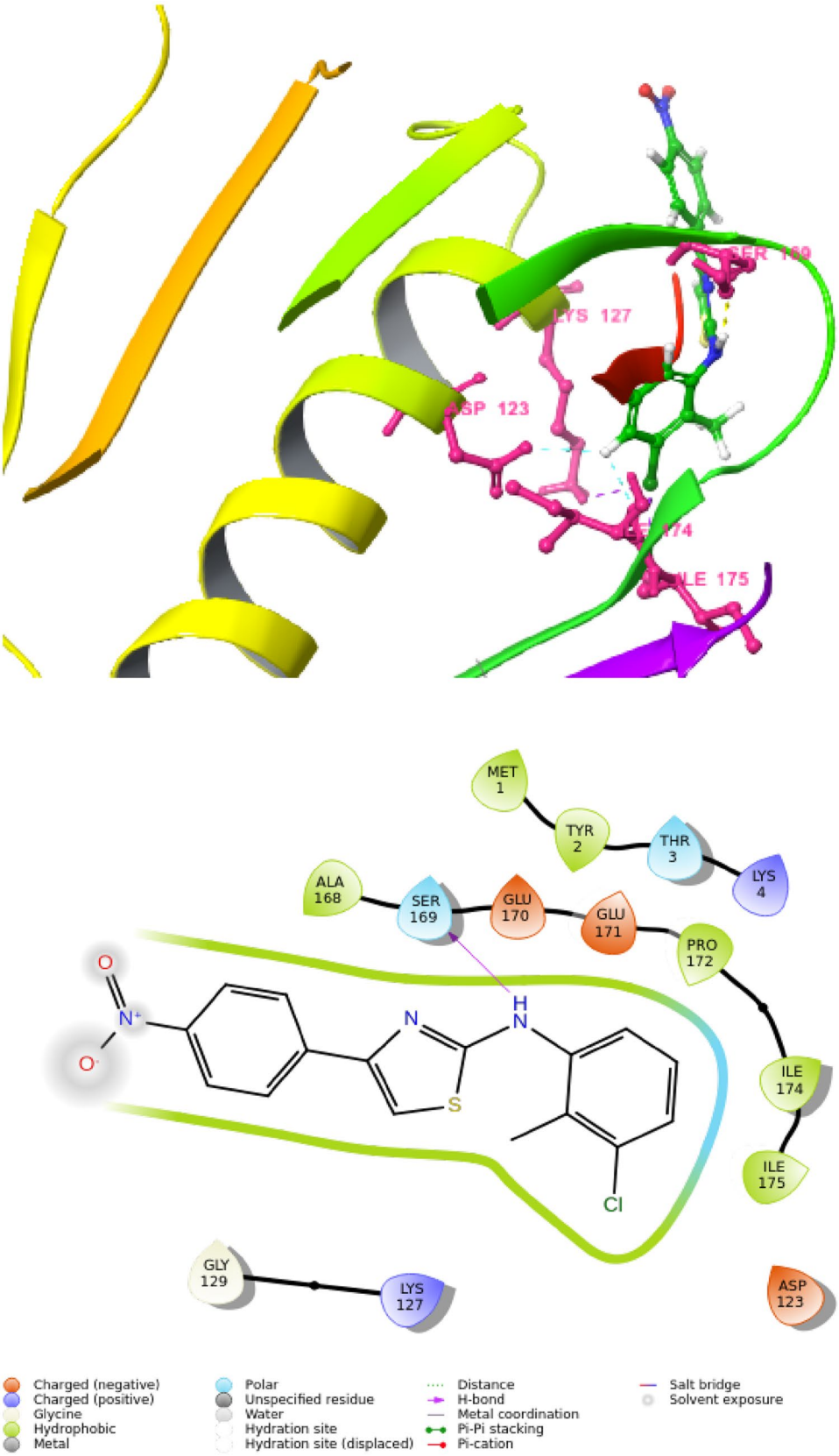

Fig. 10 Docking pose of the compound **5e** with *E. coli* FabH (PDB Id-5BNR)

Table 4 Bonds, hydrophobic interactions and D-scores of the synthesized compounds

	Compounds	H-bonds	π–π or π–cation bonds	Aromatic, Halogen bonds	Hydrophobic interactions	D-score (kcal mol^{-1})
5a	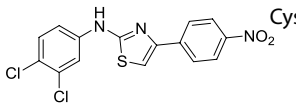	Cys^{112}, Asn^{247}		Arg^{36}, Asn^{210}	Ile$^{156, 250}$, Ala^{221,216}, Phe$^{304, 392}$, Val$^{217, 304}$	**−6.214**
5b	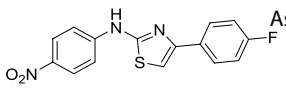	Asn^{274}, Cys^{112}	Arg^{249}	Gly^{209}	Ile^{250}, Ala$^{246, 208}$, Phe$^{213, 304}$, Met^{207}, Val^{212}, Gly$^{152, 209}$, Leu^{248}, Trp^{32}	**−5.774**
5c	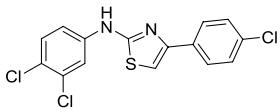		Met^{1}	Ile^{174}, Asp^{123}, Lys^{127}, Met^{1}	Ile^{174}, Ala$^{167, 168}$, Met^{1}	**−5.838**
5d	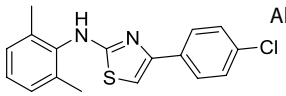	Ala^{246}		Gly^{152}	Ile$^{155, 156, 250}$, Phe^{157}, Phe$^{213, 304}$, Trp^{32}, Ala^{143}, Met^{207}, Leu^{142}	**−6.648**
5e	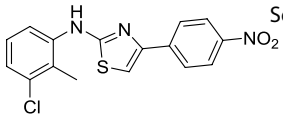	Ser^{169}		Ile^{175}, Asp^{123}, Lys^{127}	Ile$^{5, 174}$, Met^{1}, Pro^{172}, Gly^{173}	**−5.862**
5f	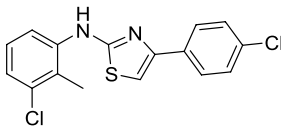		Arg^{249}	Cys^{112}, Gly^{209}	Val$^{212, 215}$, Phe^{157}, Phe$^{213, 304}$, Gly^{209}, Ile$^{155, 156}$, Val$^{215, 217}$, Ala^{216}	**−6.455**
5g	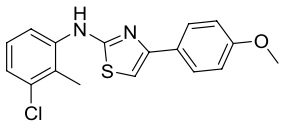		Arg^{249}	Gly^{209}, Cys^{112}	Trp^{32}, Phe$^{157,213, 304, 308}$, Gly$^{209, 305}$, Ile^{156}, Ala^{216}, Val$^{212, 215}$	**−6.413**
5h	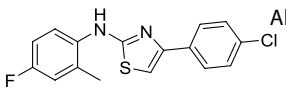	Ala^{246}, Asn^{247}	Arg^{249}, His^{244}	Arg^{36}, Gly^{209}	Trp$^{32, 304, 310}$, Phe$^{157, 213}$, Val$^{215, 217}$, Gly^{152}, Gly^{305}, Ala^{216}, Ile$^{156, 250}$	**−6.226**
5i	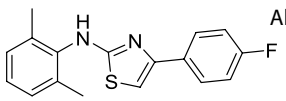	Ala^{246}	Arg^{249}	Gly^{209}	Gly^{305}, Ala^{216}, Phe$^{157, 213, 304}$, Val$^{212, 215, 217}$, Trp^{32}, Ile$^{155, 156}$	**−6.407**
5j	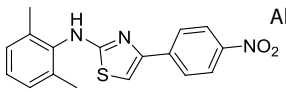	Ala^{246}, Arg^{36}	Arg^{249}	Thr^{153}	Ile$^{155, 250}$, Phe$^{157, 213, 304}$, Gly^{152}, Leu^{142}, Trp^{32}	**−6.642**

D-score is in bold to emphasize the binding affinity of the ligand and the protein

Here, T is the trajectory time over which the RMSF is calculated, t_{ref} is the reference time; r' is the position of the atom i at time t after superposition on the reference frame.

Throughout this simulation, the protein secondary structure elements (SSE) were checked. Alpha-helices (red colour) and beta-strands (blue colour) are observed. Each and every trajectory frame of SSE is summarized in the Fig. 14. The plot below explains deeply the residues index distribution in the structure of the protein Fig. 15.

The Ligand Root Mean Square Fluctuation (L-RMSF) is useful for characterizing local change with the ligand chain showing the flexibility of each residue (Figs. 16, 17, 18).

The RMSF for atom i is:

$$RMSF_i = \sqrt{\frac{1}{T}\sum_{t=1}^{T}(r_i'(t)) - (r_i(t_{ref}))^2}$$

Here, t is the trajectory time over which the RMSF is calculated, t_{ref} is the reference time; r' is the position of the atom i at time t after superposition on the reference frame.

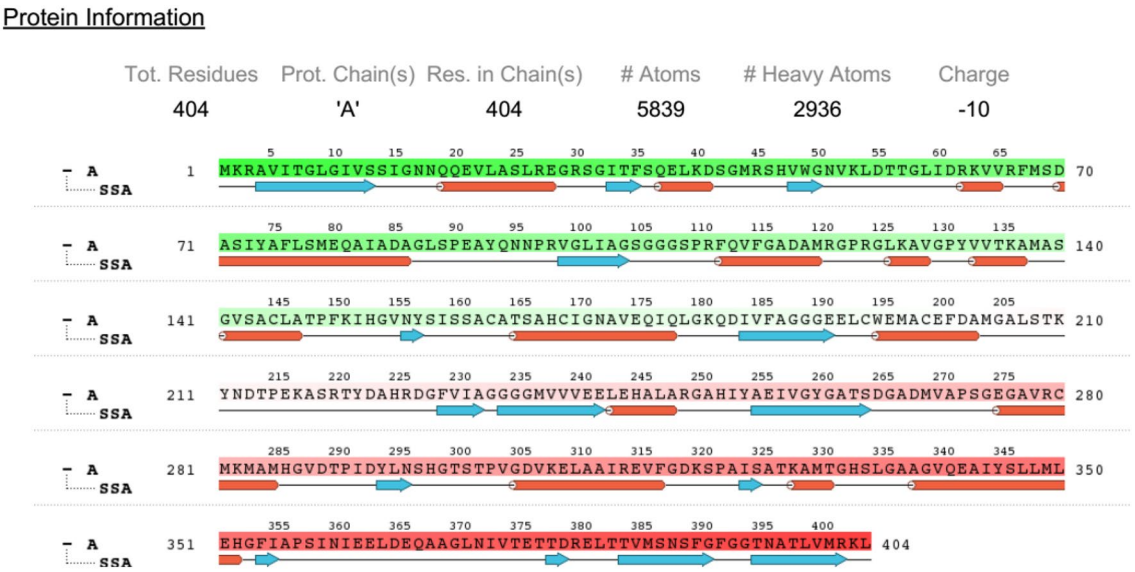

Fig. 11 Protein information

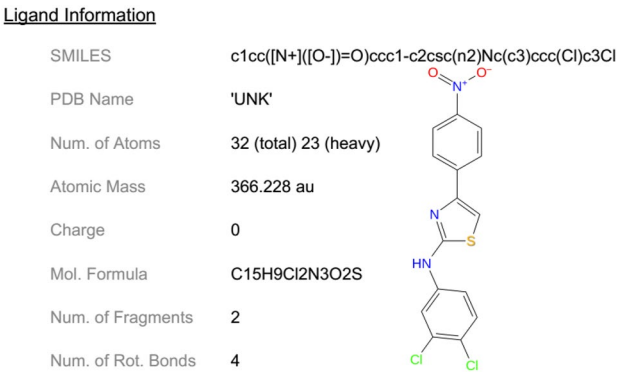

Fig. 12 Ligand information

The ligand RMSF gives the intuitions on how the ligand and protein interact as well as their entropic role and binding event. In the Fig. 19, with respect to the protein, the ligand fluctuations are shown in the 'Fit Ligand on the Protein line.

Protein–ligand interactions were checked throughout the simulation and were having four categories such as hydrogen bonds, hydrophobic, ionic and water bridges. Simulation Interaction Diagram' panel below showed interactions fractions over the course of the trajectory, for example, a value of 0.7 suggests that 70% of the simulation time and the specific interaction was maintained (Figs. 20, 21).

Fig. 13 Protein–ligand RMSD

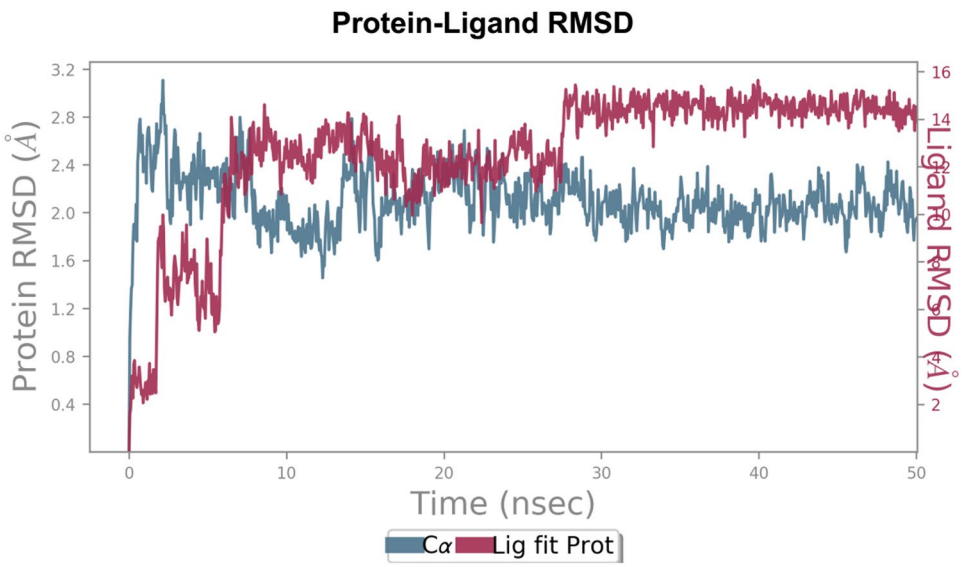

Fig. 14 Protein RMSF

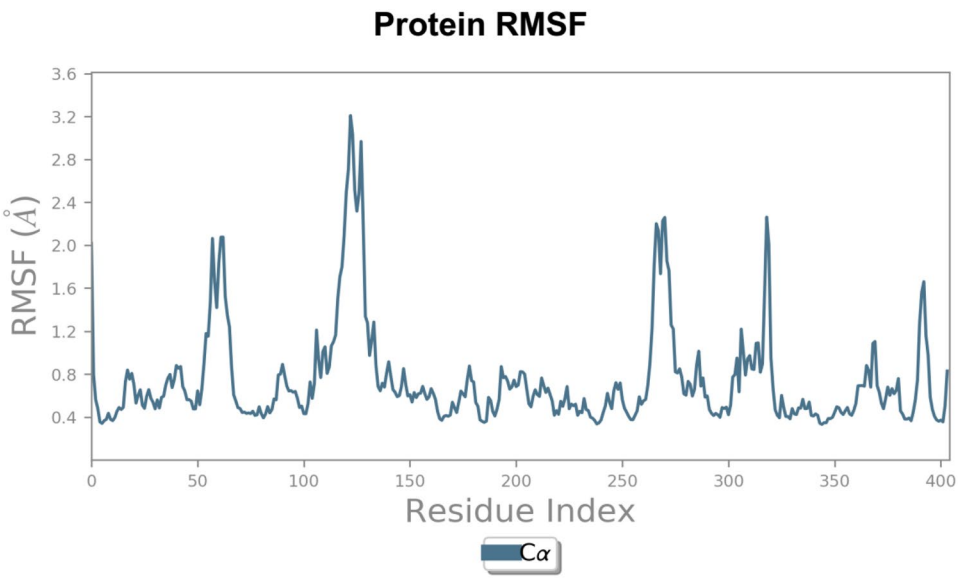

Fig. 15 Protein secondary structure

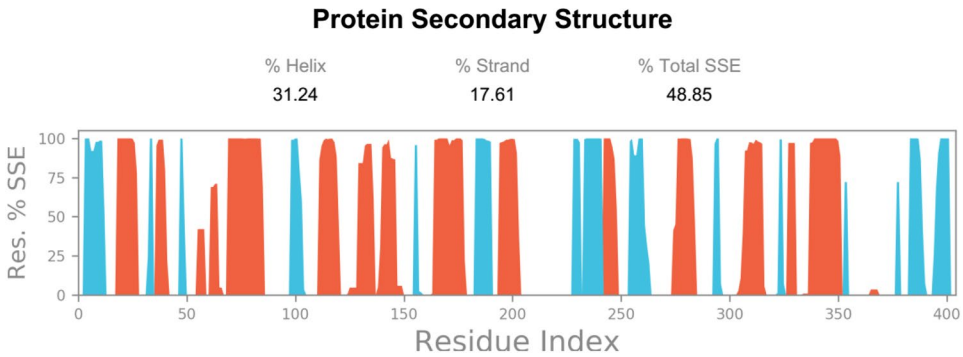

Hydrogen bonds complex stability is the must and this is provided by hydrogen bonds. The affinity of the ligand on the protein is shown by hydrogen bonds. However, hydrogen-binding property is very important in drug design because of its specificity in drug metabolization and adsorption.

Hydrophobic contacts these complain π–cation, π–π, and other no specific interactions.

Ionic interactions these characterize between two oppositely charged atoms.

Water bridges are hydrogen-bonded protein–ligand interactions mediated by a water molecule.

The Fig. 22 showed ligand–protein contact and indicated more than 30% of interactions meaning that the amino acid residues can H-bond with H-bond acceptor of the ligand. This trajectory was done through 50 nsec (Figs. 23, 24).

Ligand RMSD Here, we see the Root mean square deviation of the ligand with respect to the reference conformation.

Radius of gyration (rGyr) it helps in exhibition of conformational stability and the smaller the value of the radius of gyration, the better folding of the molecule. This stability is maintained by the constancy of the said radius.

Intramolecular hydrogen bonds (intraHB) Number of internal hydrogen bonds (HB) within a ligand molecule, here they were not detected.

Molecular surface area (MolSA) Molecular surface calculation with 1.4 Å probe radius which is value of equivalent to a van der Waals surface.

Solvent accessible surface area (SASA) Surface area of a molecule accessible by a water molecule.

Polar surface area (PSA) Solvent accessible surface area in a molecule contributed only by oxygen and nitrogen atoms.

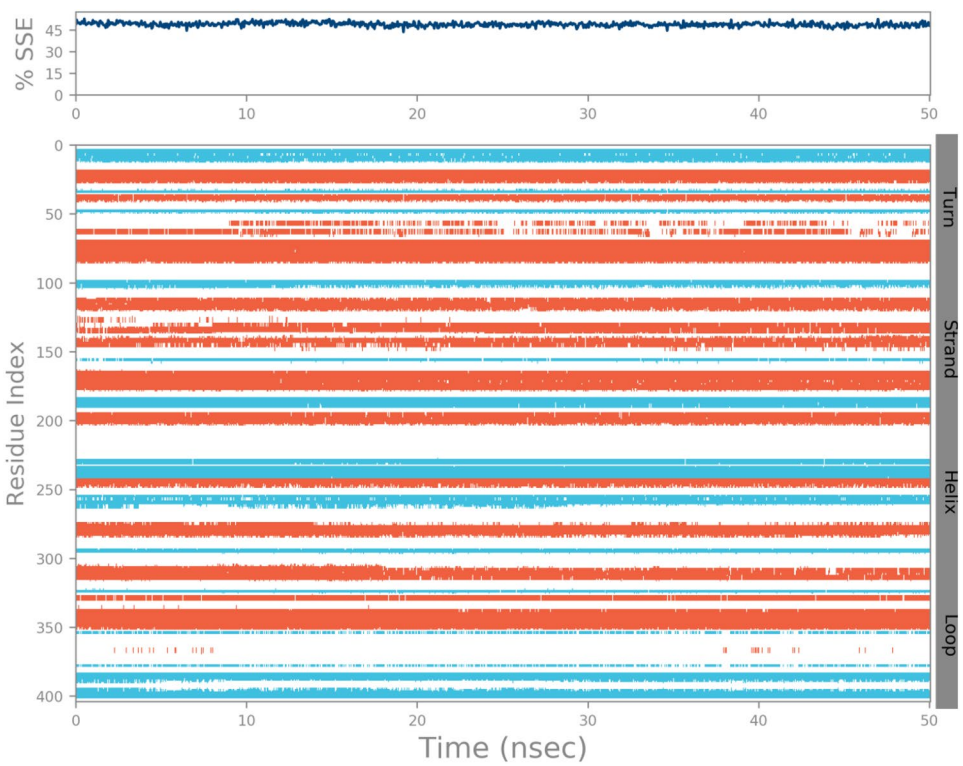

Fig. 16 The residues index distribution in the structure of the protein

Generally, Cys–Hie–Asn triad tunnel is the catalytic active site of FabH. Since this triad is conserved in bacteria and plays a significant role in chain elongation regulation and substrate binding, any interaction between the said triad and substrate revealed an important role in substrate-binding [25]. The potency of the compounds is explained by their interactions with Cys^{112}, Hie^{244} or Asn^{247} residues of the proteins FabH. Studies on *E. coli* FabH confirmed that Hie^{244} and Asn^{247} are required for decarboxylation and Cys^{112} is essential in transacylation [26]. Thiolactomycin has shown its efficacy to inhibit fatty acid synthase system but not acetyl-CoA carboxylase. Since some of our compounds were having interactions with Hie^{244} or Asn^{247}; this might explain their potency on acetyl-CoA carboxylase as they were required in decarboxylation of the mentioned protein. In addition to this, all the synthesized compounds had many good interactions with hydrophobic amino acids. The docking results with the synthesized compounds revealed that they fit well into the binding-site, display favourable interactions with the crucial amino acid residues of *E. coli* FabH and suggest good affinity for the enzyme. However, the potency of the compound **5a** was mentioned in *E. coli* by reducing the content of fatty acids. This is a serious issue since *E. coli* is known to cause idiopathic epilepsy by its capability of penetrating blood–brain–barrier (BBB). *E. coli* β-ketoacyl-ACP synthase (KAS) I which contributes to thiolactomycin resistance in *E. coli* was inhibited as shown by in silico results. This enzyme is essential for bacterial survival as it is involved in fatty acid biosynthesis. The in vitro results showed that compounds are effectively inhibiting all the essential fatty acids required for bacterial cell wall construction since they can completely inhibit the function of arachidonic acids.

The synthesized compounds can be divided by two rings: ring A and ring B, each ring possesses at least either halogen atom or nitro group. Compound **5a** has two chlorine atoms on ring A and one nitro group on ring B, having interactions with Asn^{274} and Cys^{112}, makes it promising antibacterial drugs as shown by in vitro and in silico studies on *E. coli* FabH. This is clearly explained by its in vitro antibacterial capacity. Compound **5b** has nitro group on ring A, fluorine atom on the ring B and, it showed interaction with Asn^{274} and Cys^{112}. As the compounds **5a** and **5b** showed the interaction with Cys^{112} and Asn^{247} which were two amino acids of the said triad, their ability in inhibition could be confirmed by the fatty acid inhibition results. However, all the synthesized compounds have many hydrophobic interactions with the mentioned protein. Hydrophobic interactions

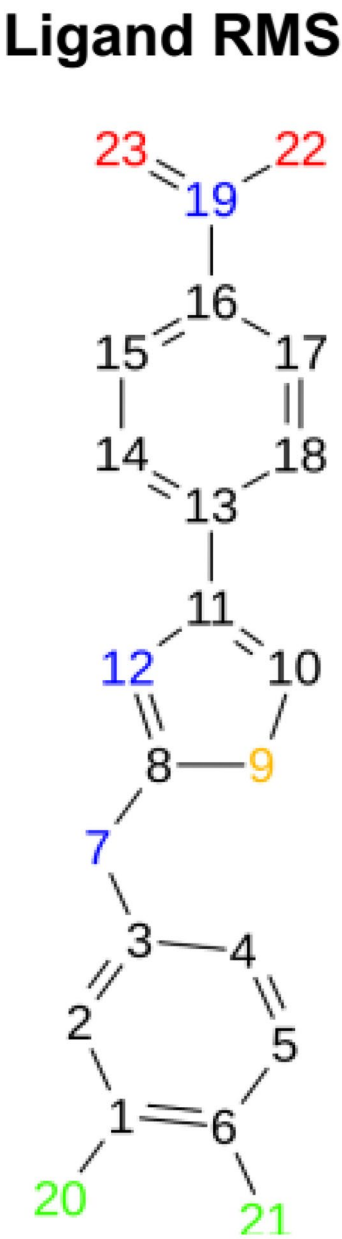

Fig. 17 Ligand RMSF

make a large contribution to the stability of the protein structure. Having hydrophobic interactions can alter the protein stability as well as activity. In general, all the synthesized compounds have minimal activity on the rest of tested microorganisms.

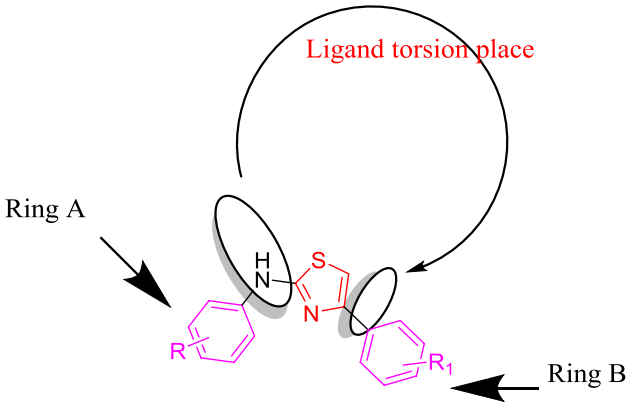

4 Conclusions

New aminothiazole derivatives were well designed synthesized and screened for their antibacterial activities. Their structure was assigned by analytical and spectroscopic techniques such as NMR, FT-IR and LCMS. The structure of the compound **5d** was supported by single crystal XRD results. The ten novel synthesized thiazole derivatives showed promising potency against the tested bacterial microorganisms. The compounds (**5a**, **5b**, **5c**, **5d**, **5e** and **5i**) were potent against *E. coli* (MTCC 443), while compounds (**5a**, **5e**, **5f** and **5i**) showed promising potency against *C. violaceum* MCC 2216. Compounds **5a**, **5e**, **5g** and **5h** showed potent activity against *E. faecalis* MTCC 2729. The potency of the mentioned compounds against *E. coli* (MTCC 443) was confirmed by in silico studies against *E. coli* FabH (PDB ID-5BNR). However none of tested compounds were potent enough to inhibit the growth of *S. Aureus* (MCC 2043). Among all tested compounds, the compound **5a** was the most potent one against all tested strains with MIC of 5.33 µM which was comparable with

Fig. 18 The ligand fluctuations

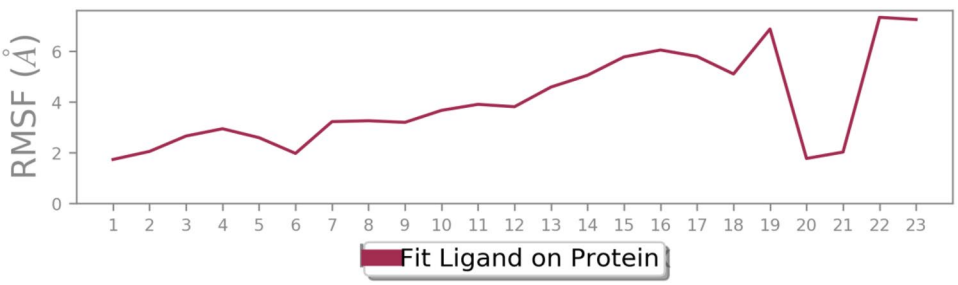

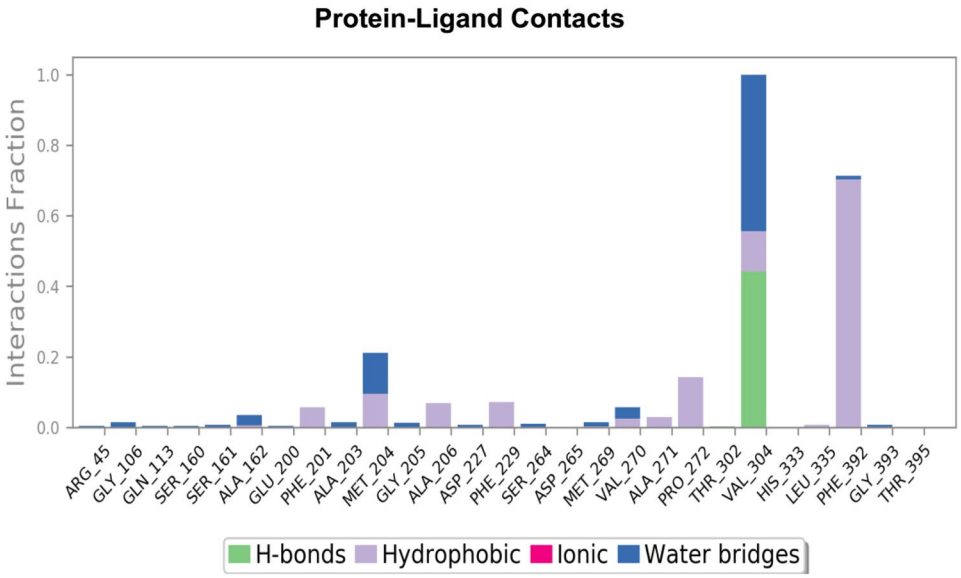

Fig. 19 Protein–ligand contacts

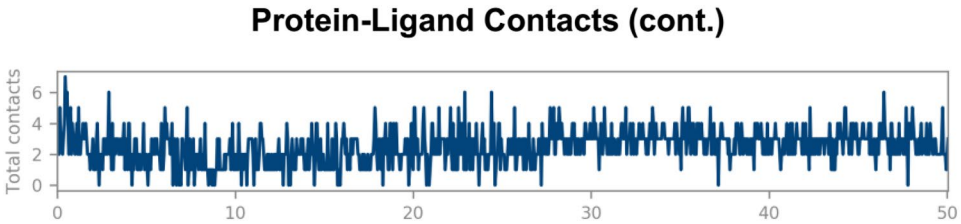

Fig. 20 Protein–ligand contacts (cont.)

standard streptomycin. Molecular docking results of the title compounds showed many interactions of them with the *E. coli* β-ketoacyl-ACP synthase (KAS) I which contributes to thiolactomycin resistance in *E. coli*. This enzyme is essential for bacterial survival as it is involved in fatty acid biosynthesis. The in vitro fatty acids inhibition results showed that compounds are effectively inhibiting all the essential fatty acids required for bacterial cell wall construction since they can completely inhibit the function of arachidonic acids. It is well understood that *E. coli* even penetrates blood–brain barrier [27], hence its capacity of generating idiopathic epilepsy [28]. In silico results complemented in vitro study results. All the tested compounds were found to possess minimum toxicity towards human blood cells. Molecular dynamic simulations done for the compound **5a** emphasized the affinity as well as the stability of the ligand with the protein during contact.

5 Experimental sections

All required reagents were used as received from suppliers without further purification. The melting point was measured in open capillary tube and correction is not applied. The IR-spectrum was recorded on Shimadzu FT-IR Prestige-21 spectrophotometer in ATR mode and is expressed in cm^{-1}. The mass spectrum was obtained using Shimadzu LC MS-8030 mass spectrometer operating at 70 eV. The ^{1}H NMR and ^{13}C NMR spectra were recorded on a Bruker AVANCE II 400 MHz instrument in $CDCl_3$/DMSO-d_6 solvent and TMS as an internal standard. The purity of the compound and completion of the reaction were monitored by TLC using Merck silica gel 60 F_{256} coated Aluminum with petroleum ether: ethyl acetate (8:2) as mobile phase. Elemental analysis was carried out.

5.1 General procedure for the synthesis of title compounds 5a–j

Equimolar amounts of substituted phenylthioureas **2** (0.01 M) and 4-substituted phenacylbromides **4** (0.01 M) in 30 mL ethanol was heated under reflux for 24 h. The TLC (ethyl acetate/petroleum ether, 8:2) was used to confirm the completion of the reaction. After cooling, separated solid was filtered, dried and recrystallized from ethanol to yield compounds **5a**–**j**. The spectral data confirming the identity of the synthesized compounds are given below.

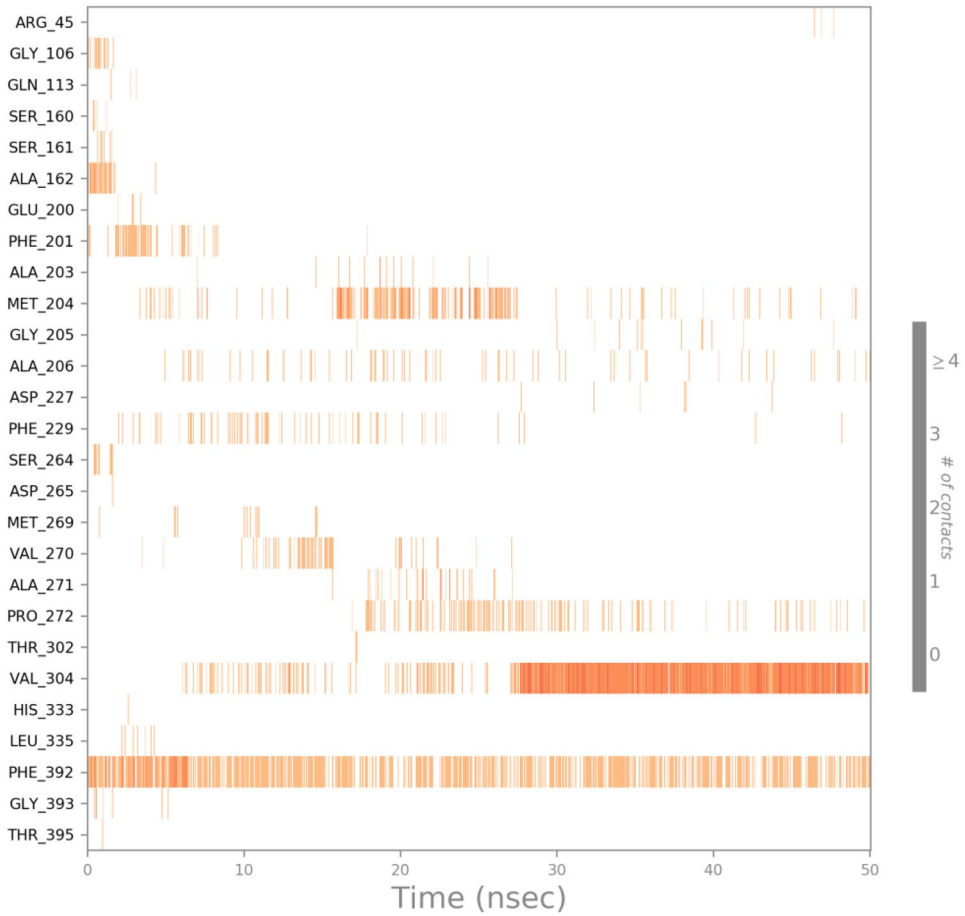

Fig. 21 The Figure 21 clearly showed that the contact is maintained and is showed by a darker shade of orange colour. From the figure above, we can detect more than 6 specific contacts which are Phe[392], Val[304], Met[204], Phe[201], Ala[162] and Gly[106]

5.1.1 N-(3,4-Dichlorophenyl)-4-(4-nitrophenyl) thiazol-2-amine (5a)

Orange solid, MP: 180–182 °C; Yield: 65%. IR (KBr, vcm^{-1}): 3126 (NH stretch), 3047 (C–H stretch), 1616 (C=C), 1552 (N–O asym stretch), 1494 (C=N), 1319 (N–O sym. stretch), 725 (C–Cl).^{1}HNMR (400 MHz, DMSO-d_6): δ (ppm) 7.62–7.65 (d, $J=8$ Hz, ortho protons of 4-NO_2-phenyl); 8.24–8.26(d, $J=8$ Hz, meta protons of 4-NO_2-phenyl), 8.11–8.13 (d, $J=8$ Hz, ortho proton of 3,4-dichlorophenyl), 8.17 (s, ortho proton of 3,4-dichlorophenyl ring), 7.47 (s, thiazole proton), and the exocyclic NH proton appeared at δ (ppm) 10.58 as a singlet. ^{13}CNMR (100 MHz, DMSO-d_6, δ ppm):162.7, 148.1, 146.2, 140.6, 131.3, 130.2, 126.2, 123.7, 122.6, 118.0, 116.7 and 107.8). Elemental analysis: Anal. Calcd.C, 49.20; H, 2.48; N, 11.47. Found: C, 49.25; H, 2.46; N, 11.48; LCMS: (m/z): $C_{15}H_8N_3Cl_2O_2S$: 366.00 $(M+H)^+$, 368.00 $(M+H+2)^+$, 370.00 $(M+H+4)^+$.

5.1.2 4-(4-Fluorophenyl)-*N*-(4-nitrophenyl) thiazol-2-amine (5b)

Orange solid, MP: 180–182 °C; Yield: 65%. IR (KBr, vcm^{-1}): 3130 (NH stretch), 3045 (C–H stretch), 1094(C=N), 1616 (C=C), 1554 (N–O asym stretch), 1319 (N–O sym stretch), 1056 (C–F). ^{1}H-NMR (400 MHz, DMSO-d_6): δ (ppm) 7.12–7.14 [2H, d, ($J=8$ Hz), ortho protons of 4-nitrophenyl]; 8.17–8.19 [(2H, d ($J=8$ Hz) meta protons of 4-nitrophenyl]; 7.90–7.93 [2H, dd ($J=12$ Hz, $J=4$ Hz) (HF ortho) meta protons 4-fluorophenyl], 7.93–7.95 [2H, dd [$J=8$ Hz, $J=4$ Hz) (HF meta) 4-fluorophenyl ring],and the exocyclic NH proton appeared at δ (ppm) 10.94 as a singlet. ^{13}CNMR (100 MHz, DMSO-d_6, δ ppm): 161.8, 151.4, 149.7, 146.9, 140.3, 127.7, 125.6, 116.1, 115.4 and 114.1. Elemental analysis: Calcd.C, 57.14; H, 3.20; N, 13.33. Found: C, 57.15; H, 3.19; N, 13.34.). LCMS: (m/z): $C_{15}H_{10}N_3FO_2S$: 356.05 $(M+H)^+$.

5.1.3 4-(4-Chlorophenyl)-*N*-(3,4-dichlorophenyl) thiazol-2-amine (5c)

Lemon yellow solid, MP: 118–120 °C; Yield: 65%. IR (KBr, vcm^{-1}): 3178 (NH stretch), 3039 (C–H stretch), 1632 (C=N), 725 (C–Cl). ^{1}H-NMR (400 MHz, DMSO-d_6): δ (ppm) 7.26 (thiazole), 7.88–7.90 (d, 2H, $J=8$ Hz, ortho protons of -4-chlorophenyl ring); 7.43–7.40(d, 2H, $J=12$ Hz, metaprotons of 4-chlorophenyl ring), 8.09–8.10 (d, 1H, $J=4$ Hz, ortho proton of 3,4-dichlorophenyl ring), 7.45 (s, ortho proton of

Fig. 22 Ligand–protein contact

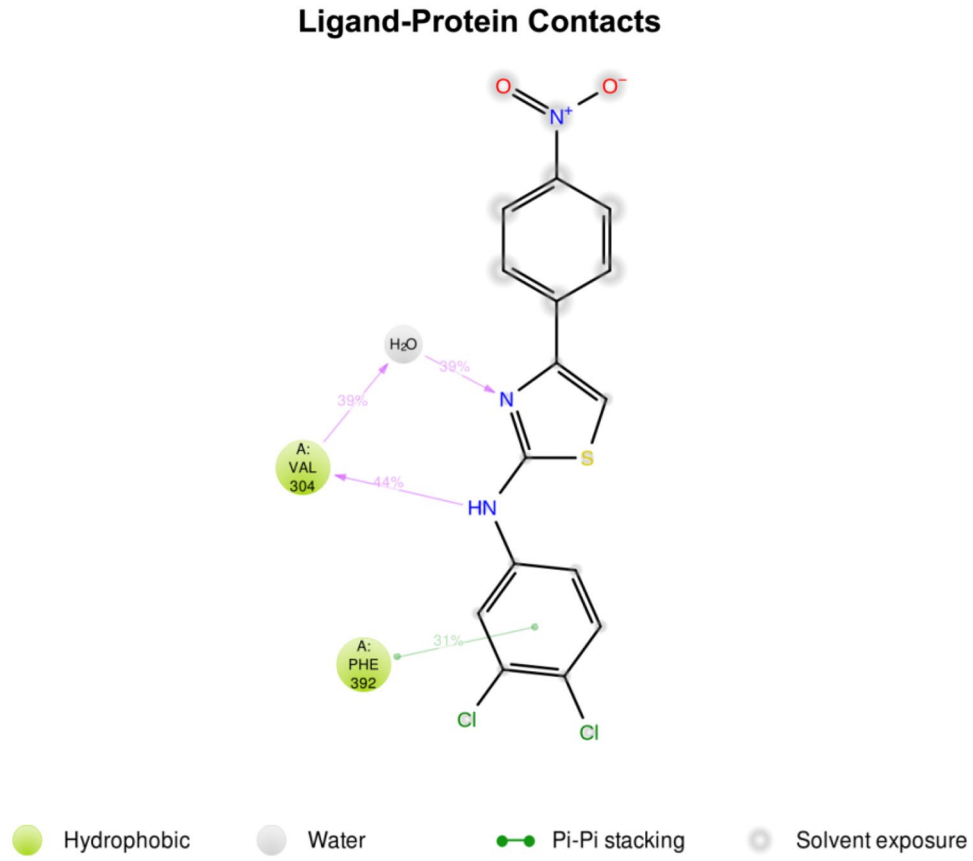

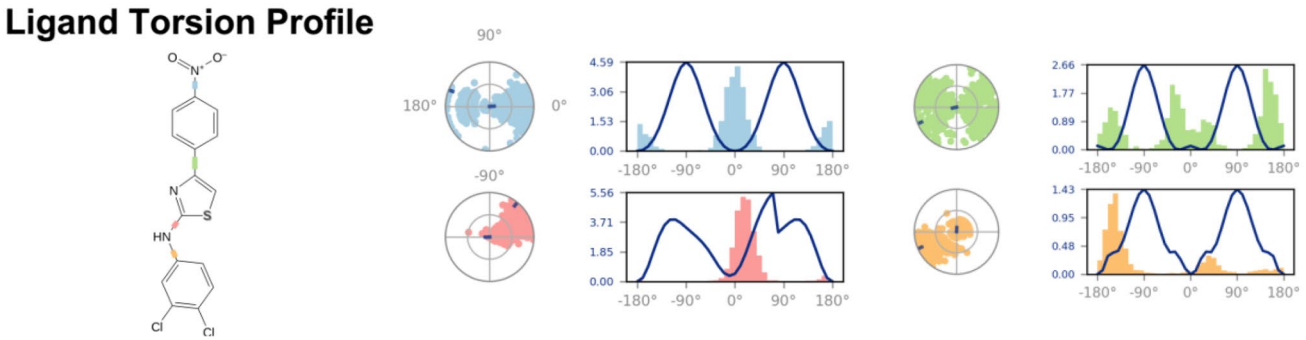

Fig. 23 The figure 23 shows the rotatable bond in the ligand, on left Y-axis is the potential expressed in Kcal/mol and the torsion potential relationship gives awareness into the conformational strain the ligand is undergoing to keep a protein- bond conformation

3,4-dichlorophenyl ring), 7.60–7.63 [dd, (J = 12 Hz, J = 4 Hz, (meta proton of 3,4-dichlorophenyl ring)], and the exo-cyclic NH proton appeared at δ (ppm) 10.45 as a singlet. ^{13}CNMR (100 MHz, DMSO-d_6, δ ppm):162.4, 148.9, 140.8, 133.0, 132.2, 131.3, 130.2, 128.4, 127.0, 122.3, 117.9, 116.6 and 103.9. Elemental analysis: Calcd: Anal. Calcd.C, 49.20; H, 2.48; N, 11.47. Found: C, 49.21; H, 2.47; N, 11.48. LCMS: (m/z): $C_{15}H_9N_2Cl_3S$: 355.85 $(M+H)^+$, 357.85 $(M+H+2)^+$, 359.85 $(M+H+4)^+$, 361.85 $(M+H+6)^+$.

5.1.4 *N*-(2,6-Dimethylphenyl)-4-(4-chlorophenyl) thiazol-2-amine (5d)

Greyish white solid, MP: 220–222 °C; Yield: 65%. IR (KBr, vcm^{-1}): 3143 (NH stretch), 3043 (Ar–H stretch), 2929 (C–H alkyl stretch), 1573 (C=C), 1184 (C=N), 729 (C–Cl). ^{1}HNMR (400 MHz, DMSO-d_6): δ (ppm) 6.63 (Ar–H-thiazole), 7.66–7.68 (d, 2H, J = 8 Hz, ortho protons of 4-chlorophenyl); 7.25–7.28 (d, 2H, J = 8.8 Hz, meta protons of 4-chlorophenyl ring), 7.20–7.21 (d, 2H, J = 4 Hz, meta proton

Fig. 24 Ligand properties

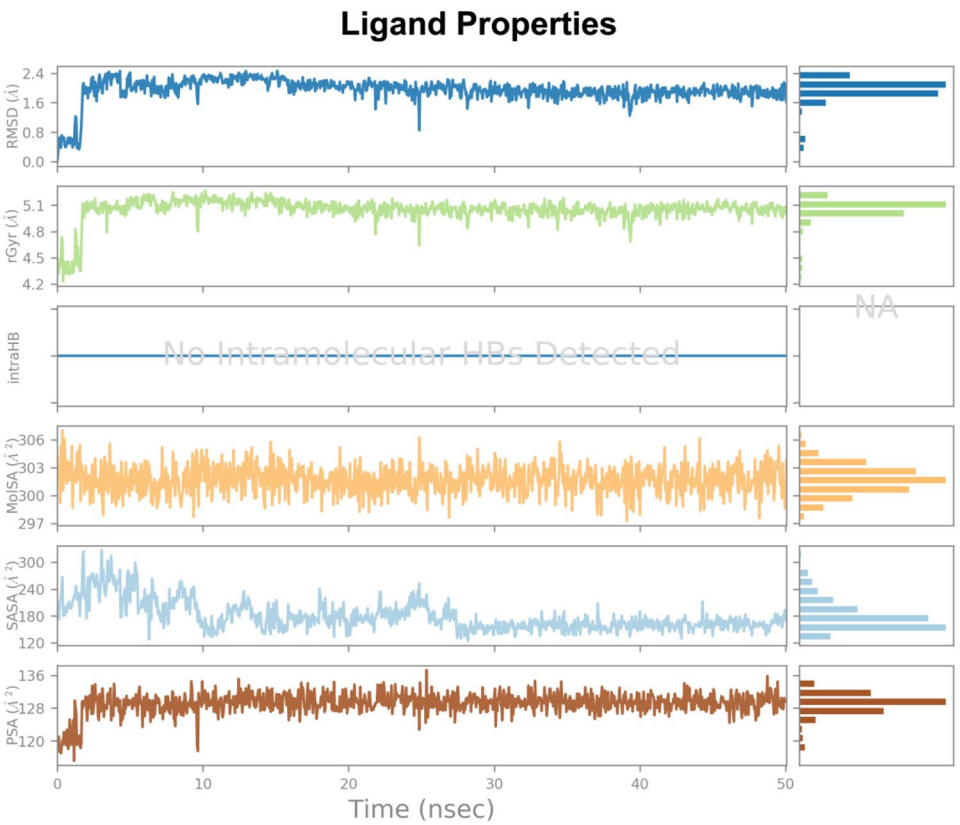

of 2,6-methylphenyl ring), 7.19–7.20 (d, 1H, $J = 4$ Hz, 1H, meta proton of 2,6-dimethylphenyl ring), 7.17–7.16 (d, Ar–H, $J = 4$ Hz; para proton of 2,6-dimethylphenyl ring), 2.32 (s, 6H, alkyl.^{13}CNMR (100 MHz, DMSO-d_6, δ ppm): 168.4, 149.1, 137.7, 135.9, 133.4, 131.8, 128.2, 127.0, 126.7, 101.8 and 17.9. Elemental analysis: Anal. Calcd.C, 64.86; H, 4.80; N, 8.90. Found: C, 64.85; H, 4.81; N, 8.89. LCMC: (m/z):$C_{17}H_{15}N_2ClS$:315.00 $(M+H)^+$, 317.00 $(M+H+2)^+$.

5.1.5 *N*-(3-Chloro-2-methylphenyl)-4-(4-nitrophenyl) thiazol-2-amine (5e)

Yellow solid, MP: 180–182 °C; Yield: 65%. IR (KBr, vcm^{-1}): 3130 (NH stretch), 3039 (Ar–H stretch), 2860 (C–H alkyl stretch),1618 (C=C), 1554 (N–O asym stretch), 1494 (C=N), 1319 (N–O sym stretch),725 (C–Cl).^{1}H-NMR (400 MHz, DMSO-d_6): δ (ppm) 9.61 (s, N–H), 7.59 (s, 1H thiazole), 8.08–8.10 [d, ($J = 8$ Hz, ortho protons of 4-nitrophenyl ring)]; 8.21–8.23 [(d, ($J = 8$ Hz) meta protons of 4-nitrophenyl ring]; 8.25 [s, para proton of 2-methyl-3-chlorophenyl ring), 7.94–7.96 (d, $J = 8$ Hz, ortho proton of 2-methyl-3-chlorophenylring), 7.17–7.23 (dd, $J = 24$ Hz, J = 8 Hz, meta proton of 2-methyl-3-chlorophenyl ring). ^{13}CNMR (100 MHz, DMSO-d_6, δ ppm): 165.5, 147.8, 146.1, 140.5, 134.1, 127.2, 126.8, 124.1, 123.7, 120.0, 107.6 and 14.8. Elemental analysis: Anal. Calcd. C, 55.57; H, 3.50; N, 12.15. Found: C, 55.58; H, 3.48; N, 12.14. LCMS: (m/z): $C_{16}H_{12}N_3ClO_2S$: 346.00 $(M+H)^+$, 348.00 $(M+H+2)^+$.

5.1.6 *N*-(3-Chloro-2-methylphenyl)-4-(4-chlorophenyl) thiazol-2-amine (5f)

White solid, MP: 200–202 °C; Yield: 65%. IR (KBr, vcm^{-1}): 3130 (NH stretch), 3039 (Ar–H stretch), 2926(C–H alkyl stretch), 1494 (C=N), 1618 (C=C), 1056 (C–F). ^{1}H-NMR (400 MHz, DMSO-d_6): δ (ppm), 7.93–7.95 [dd, ($J = 16$ Hz, $J = 8$ Hz, H–Cl ortho) meta protons of 4-chlorophenyl ring)]; 7.84–7.85 [(d, ($J = 4$ Hz, H–Cl meta) ortho protons of 4-chlorophenyl ring]; 7.82–7.83 (d, ($J = 4$ Hz, ortho proton), 7.13 (s, thiazol proton. 7.43–7.45 (d, $J = 8$ Hz, meta proton of 2-methyl-3-chlorophenyl ring), 7.34–7.36 (d, $J = 8$ Hz, ortho proton of 2-methyl-3-chlorophenyl ring), 2.35 (s, 3H, 4-chlorophenyl ring) and the exocyclic NH proton appeared at δ (ppm) 9.45 as a singlet.^{13}CNMR (100 MHz, DMSO-d_6, δ ppm): 166.1, 164.0, 146.1, 140.3, 134.4, 130.0, 129.9, 127.7, 126.9, 124.8, 120.7, 115.3, 114.8, 102.7 and 14.9. Elemental analysis:Anal. Calcd.C, 60.28; H, 3.79; N, 8.79. Found: C, 60.26; H, 3.80; N, 8.78. LCMS: (m/z):$C_{16}H_{12}N_2ClFS$: 319.00$(M+H)^+$, 321.00 $(M+H+2)^+$.

5.1.7 *N*-(3-Chloro-2-methylphenyl)-4-(4-methoxyphenyl) thiazol-2-amine(5g)

Off white solid, MP: 208–210 °C; Yield: 65%. IR (KBr, vcm^{-1}): 3053(NH stretch), 3053 (Ar–H), 2966 (C–H-aIkyl), 1562 (C=C), 1506(C=N), 1055 (C–O stretch), 732 (C–Cl). ^{1}H-NMR (400 MHz, DMSO-d_6): δ (ppm) 11.32 (s, N–H), 7.42–7.44(Ar–H, d, J=8 Hz, protons of 2-methyl3-chlorophenyl)]; 7.33–7.35 (d, J=8 Hz) protons of 2-methyl-3-chlorophenyl ring]; 7.23–7.25 [d, (J=8 Hz) protons of 4-methoxyphenyl ring], 7.00–7.02 [d, J=8 Hz], 4-meta protons of methoxyphenyl ring, 7.74–7.72 (2H, d, ortho 4-methoxyphenyl ring), 3.8 (s, 3H of alkyl methoxy), 2.5 (3H, s, alkyl).^{13}CNMR (100 MHz, DMSO-d_6, δ ppm): 159.2, 140.1, 139.7, 134.4, 129.1, 127.2, 113.7, 100.9 and 14.8. Elemental analysis: Anal. Calcd. C, 61.72; H, 4.57; N, 8.47. Found: C, 61.74; H, 4.55; N, 8.46. LCMS: (m/z):$C_{17}H_{15}N_2ClOS$: 331.05 $(M+H^+)$, 333.05 $(M+H+2)^+$.

5.1.8 4-(4-Chlorophenyl)-N-(4-fluoro-2-methylphenyl) thiazol-2-amine (5h)

Pale violet solid, MP: 135–137 °C; Yield: 65%; IR (KBr, vcm^{-1}): 3126 (NH), 3049 (Ar–H), 2856(C–H-alkyl), 1616 (C=C), 1496 (C=N), 1056 (C–F), 725 (C–Cl), ^{1}H NMR ($CDCl_3$, 400 MHz) δ ppm: 2.26 (s, 3H alkyl). 7.64–7.65 (d, 2H, ortho protons of 4-chlorophenylring),6.94–6.96 (d, 2H, meta protonsof 4-chlorophenyl ring), 7.66–7.67 (d, 1H, J=4 Hz, proton of 2-methyl-4-fluorophenyl ring), 7.49–7.52 (dd, 2H, J=12 Hz, J=4 Hz, meta protons of 2-methyl-4-fluorophenyl ring). ^{13}C-NMR (DMSO-d_6, 100 MHz) δ ppm: 166.2, 159.7, 157.3, 148.8, 135.5, 133.3, 132.5, 128.3, 127.1, 123.6, 116.9, 112.8, 102.8 and 18.1). Elemental analysis: Anal. Calcd. C, 60.28; H, 3.79; N, 8.79. Found: C, 60.29; H, 3.78; N, 8.80. LCMS: (m/z): $C_{16}H_{12}N_2ClFS$:318.95 $(M+H^+)$, 320.95$(M+H+2)^+$.

5.1.9 *N*-(2,6-Dimethylphenyl)-4-(4-fluorophenyl) thiazol-2-amine (5i)

Peach solid, MP: 150–152 °C; Yield: 69.29%; IR (KBr, vcm^{-1}): 3126 (NH), 3047 (Ar–H), 2856 (CH alkyl), 1616 (C=C), 1496 (C=N), 1056 (C–F), 725 (C–Cl). ^{1}H NMR ($CDCl_3$, 400 MHz) δ ppm: 2.32 (s, 6H, alkyl), 6.57 (s, thiazole), 7.21–7.13 (m, 3H, 2,6-dimethylphenyl ring),7.73–6.99 (dd, J=16 Hz, J=4 Hz, 2H of meta 4-fluorophenyl ring), 7.01–6.97 (dd, J=16 Hz, J=4 Hz, 2H of ortho 4-fluorophenyl ring). ^{13}C-NMR (DMSO-d_6, 100 MHz) δ ppm: 168.6, 162.7, 160.3, 149.4, 137.9, 136.0, 131.2, 128.3, 127.4, 126.8, 115.1, 114.9, 100.8 and 18.0. Elemental analysis: Anal. Calcd. C, 53.11; H, 2.67; N, 8.26. Found: C, 53.13; H, 2.66; N, 8.24. LCMS: (m/z): $C_{15}H_9N_2Cl_2FS$:295.05 $(M+H)^+$.

5.1.10 *N*-(2,6-Dimethylphenyl)-4-(4-nitrophenyl) thiazol-2-amine (5j)

Yellow solid, MP: 158–160 °C; Yield: 50.13%; IR (KBr, vcm^{-1}): 3169 (NH), 3051 (Ar–H), 2846 (C–H alkyl), 1595 (C=C),1504 (N–O asym stretch), 1504 (C=N), 1321 (N–O symstretch), 1056 (C–F). ^{1}H NMR ($CDCl_3$, 400 MHz) δ ppm: 2.32 (s, 6H, alkyl); 7.86 (s, Ar–H, thiazole ring); 7.21–7.15 (m, 3H, 2,6-dimethylphenyl ring); 8.14–8.12 (d, J=8 Hz, 2H of ortho 4-nitrophenyl ring), 7.87–7.85 (d, J=8 Hz, 2H of meta of 4-nitrophenyl ring).^{13}C-NMR (DMSO-d_6, 100 MHz) δ ppm: 168.7, 148.3, 145.9, 140.7, 137.5, 135.9, 128.2, 126.9, 123.5, 105.8 and 17.9. Elemental analysis: Anal. Calcd. C, 62.75; H, 4.65; N, 12.91. Found: C, 62.76; H, 4.64; N, 12.92. LCMS: (m/z): $C_{17}H_{15}N_3O_2S$: 326.00$(M+H)^+$.

5.2 Antibacterial evaluation

The resistance of biological infections on available drugs has been reported wide worldly; therefore researchers have to focus toward the new antimicrobial drugs with new target [29]. The synthesized compounds were screened in vitro for their antibacterial activity against four referential strains namely, *E. coli* MTCC 443 and *C. violaceum* MCC 2216 (Gram-negative), *S. aureus* MCC 2043 and *E. faecalis* MTCC 2729 (Gram positive),using the disc diffusion method [30]. Thus, disinfected plates were filled with 20 mL of sterilized Muller Hinton agar medium. Afterwards, 100 mL of particular bacterium which contained of 0.5–106 CFU mL (tantamount to 0.5 McFarland standards) was dispersed on the plates surfaces using a sterile swab. The discs which had been impregnated with (15 µL) the each compound with (25 mg mL^{-1} in DMSO) and were placed on the agar surface. The disc soaked in the DMSO was used as negative control. The plates were incubated at 37 °C for 24 h, and the diameter of the zones of inhibition was measured in millimetres (mm). The sample test was performed in three replicates. Compounds showing significant zone of inhibition were subjected to minimum inhibitory concentration (MIC). MICs were performed in MH Broth in 96-well microplates by a dilution method. Tantamount to 0.5 McFarland standards, exponential bacterial cultures (1.5×10^8 c.f.u) were obtained, added to wells containing decreasing concentrations of the compounds. The 96-well microplates were incubated at 37 °C overnight and the MIC was determined as the lowest concentration that inhibits the visible growth of the microorganism. The stock solution of the test compound was made with 1 mg mL^{-1} along with the standard drug streptomycin.

5.3 Fatty acid inhibition study

Fatty acid methyl esters were prepared using Metcalfe method in duplicate from bacterial isolates (100 µL) in the presence of Triheptadecanoin (internal standard); NuChek prep, Elysian, MN, USA). Using gas chromatography with flame ionization detection, four fatty acids were accounted. Individual fatty acids are expressed as percent of total acids in a sample. For all samples, data peaks on chromatograms were examined to ensure peak quality and consistency of retention times. Based on retention time of methyl ester derivatives, fatty acids in sample were recognized.

5.4 Hemolysis assay

Sashidhara et al. [31] suggested the procedure regarding this assay: The human blood was collected in a container of EDTA (2 mg mL^{-1}). The resulting suspension was centrifuged at 800×*g* for 10 min to separate buffy coat and plasma. Successively, the erythrocytes settled were washed thrice with normal saline (0.9%) and then suspended in saline to obtain 5% erythrocytes suspension. Incubation of the cells was done in 1 h at 37 °C in the presence of test compounds (100 µg mL^{-1}). Once incubation done, the solutions were centrifuged at 800×*g* for 10 min and then absorbance of the supernatant was measured using UV spectrophotometer at 540 nm. The 2% Triton X-100 (Sigma-Aldrich, St. Louis, USA) were used as positive control. The absorbance recorded for the released haemoglobin was expressed as % of Triton X-100 induced hemolysis. The result was calculated by using the formula below:

$$\%\ \text{Hemolysis} = \frac{(\text{Absorbance of the sample}) - (\text{Absorbance of blank})}{\text{Highest absorbance of positive control}} \times 100$$

5.5 Single crystal X-ray diffraction

The X-ray intensity data for compound **5d** is collected at a temperature of 296 K on a Rigaku Saturn724 diffractometer using graphite monochromated Mo-Kα radiation. A complete data set was processed using Crystal Clear [32]. The structure was solved by direct methods and refined by full-matrix least squares method on F2 using SHELXS and SHELXL programs [33, 34]. All the non-hydrogen atoms were revealed in the first difference Fourier map itself. All the hydrogen atoms were positioned geometrically (C–H = 0.93(aromatic)/0.96(methyl) Å, N–H = 0.86 Å) and refined using a riding model with Uiso (H) = 1.2 Ueq (C or N) or 1.5 Ueq(C). After ten cycles of refinement, the final difference Fourier map showed peaks of no chemical significance. The ORTEP and packing diagrams were generated using the software MERCURY [35].

6 Supplementary information for XRD

Crystallographic data for the compounds has been deposited with the Cambridge Crystallographic Data Centre as supplementary publication number CCDC 1845758. Copies of this information may be obtained free of charge via www.ccdc.cam.ac.uk/conts/retrieving.html (or from the CCDC, 12 Union Road, Cambridge CB2 1EZ, UK; fax: +44-1223-336033; e-mail: deposit@ccdc.cam.ac.uk).

Acknowledgements The authors acknowledge the services of Dr Pritesh Bhat and Vinod Devaraji, Application Scientist in molecular docking and molecular dynamic simulation studies using Schrodinger Software. The authors thank Dr. Suchetha Kumari Professor of Biochemistry, from K. S. Hedge Medical Academy (Nitte Deemed to be University) for her contribution in fatty acid study. The authors are grateful to Dr Vaishali Rai M Assistant Professor Department of Microbiology St. Aloysius College (Autonomous) Mangalore for his contribution in hemolysis assay. One of authors (Nadine Uwabagira) is also thankful to Indian Council for Culture Relations (ICCR) for granting scholarship.

Compliance with ethical standards

Conflict of interest We declare that there is no conflict of interest.

Human and animals rights No human or animal participant were involved in this study.

References

1. Ghasemi B, Sanjarani G, Sanjarani Z, Majidiani H (2015) Evaluation of anti-bacterial effects of some novel thiazole and imidazole derivatives against some pathogenic bacteria. Iran J Microbiol 5:281–286
2. Richard H, Charles R (1996) Regulation of fatty acid and initiation by acyl acyl-carrier protein in *E. coli*. J Biol Chem 271:1833–1836
3. Peng-Cheng L, Kai-Rui W, Ying Y, Wen-Jun M, Jin C, Jing X, Hai-Liang Z (2009) Design, synthesis and biological evaluation of novel thiazole derivatives as potent FabH inhibitors. Bioorg Med Chem Lett 19:6750–6754
4. Hayashi T, Yamamoto O, Sasaki H, Kawaguchi A, Okazaki H (1983) Mechanism of action of the antibiotic thiolactomycin inhibition of fatty acid synthesis of *E. coli*. Biochem Biophys Res Commun 115:1108–1113
5. Nishida I, Kawaguchi A, Yamada M (1984) Selective inhibition of type II fatty acid synthetase by the antibiotic thiolactomycin. Plant Cell Physiol 25:265–268
6. Tsay J, Charles R, Suzanna J (1992) Overproduction of β-ketoacyl-acyl carrier protein synthase. Iran J Bacteriol 174:508–513
7. Siddiqui N, Arshad F, Ahsan W, Alam S (2009) A valuable insight into the recent advances and biological activities. Int J Pharm Sci Drug Res 3:136–143

8. Nayak SP, Narayana B, Sarojini BK, Hedge K, Shashidhara SK (2014) Design and synthesis of novel heterocyclic acetamide derivatives for potential analgesic, anti-inflammatory, and antimicrobial activities. Med Chem Res 23:4280–4294
9. Madni M, Hameed S, Ahmed N, Tahir N, Al-Masoudi A, Pannecouque C (2017) Synthesis, in vitro α-glucosidase inhibitory activity and molecular docking studies of new thiazole derivatives. Med Chem Res 26:2653–2665
10. Garuti L, Roberti M, Pession A, Leoncini E, Hrelia S (2001) Synthesis and antiproliferative activity of some thiazolylbenzimidazole-4,7-diones. Bioorg Med Chem Lett 11:3147–3149
11. Sadek B, Al-Tabakha M, Fahelelbom S (2011) Antimicrobial prospect of newly synthesized 1,3-thiazole derivatives. Molecules 16:9386–9396
12. Prakasha K, Raghavendra G, Harsha R, Channe D (2011) Design, synthesis and antimicrobial screening of amino acids conjugated 2-amino-4-arylthiazole derivatives. Int J Pharm Pharm Sci 3:120–125
13. Zhao M, Yin Y, Yu X, Sangani C, Wang S, Lu A, Yang L, Lv P, Jiang M, Zhu H (2015) Synthesis, biological evaluation and 3D-QSAR study of novel 4,5-dihydro-1H-pyrazole thiazole derivatives as $BRAF^{V600E}$ inhibitor. Bioorg Med Chem Lett 23:46–54
14. Praveen SA, Yathirajan SH, Narayana B, Sarojini BK (2014) Synthesis, characterization and antimicrobial studies of a few novel thiazole derivatives. Med Chem Res 23:259–268
15. Hargrave K, Hess F, Oliver J (1983) *N*-(4-Substituted-thiazolyl) oxamic acid derivatives, a new series of potent, orally active antiallergy agents. J Med Chem 26:1158–1163
16. Jaen J, Wise L, Caprathe B, Tecle H, Bergmeier S, Christine H, Humblet C, Heffner T, Meltzer L, Pugsley T (1990) 4(-1,2,5,6Tetrahydro-1-alkyl-3- pyridinyl-2 thiazolamines as novel class of compounds with central dopamine agonist properties. J Med Chem 33:311–317
17. Parrino B, Attanzio A, Spano V, Cascioferro S, Montarbano A, Barraja P, Tesoriere L, Diana P, Cirrincione G, Carbone A (2017) Synthesis, antitumor activity and CDK-1 inhibitor of new thiazole nortopsentin analogues. Eur J Med Chem 138:371–383
18. Zheng L, Qiu Q, Xu X, Wang X, Jiao L, Su X, Pan M, Huang W, Qian H (2016) Design, synthesis and structure-activity relationship studies of new thiazole-based free fatty acid receptor 1 agonists for the treatment of type 2 diabetes. Eur J Med Chem 113:246–257
19. Mashima T, Seimiya H, Tsuruo T (2009) De novo fatty acid synthesis and related pathway as molecular targets for cancer therapy. Br J Cancer 100:1369–1372
20. Tsay J, Oh W, Larson T, Jackowski S, Rock S (1992) Isolation and characterization of the β-ketoacyl carrier protein synthase III gene FabH from *E. coli* K-12. J Biol Chem 10:6807–6814
21. Clough R, Matthis A, Barnum S, Jaworsk J (1992) Purification and characterization of β-ketoacyl acyl carrier protein synthase III from spinach. J Biol Chem 267:20992–20998
22. Richard H, Charles R (1996) Overproduction of β-ketoacyl-acyl carrier protein synthase I imparts thiolactomycin resistance to *Escherichia coli* K-12. J Biol Chem 271:1833–1836
23. Yavari I, Hossaini Z, Sabbaghan M, Ghazanfarpour DM (2009) A one-pot synthesis of functionalized thiazoles from acid chlorides, secondary amines, ethyl bromopyruvate, and ammonium thiocyanate. Mol Divers 13:295–300
24. Holla S, Malini V, Rao S, Sarojini BK, Kumari S (2003) Synthesis of some new 2,4-disubstituted thiazoles as possible antibacterial and anti-inflammatory agents. Eur J Med Chem 38:313–318
25. Huang W, Jia J, Edwards P, Dehesh K, Schneider G, Lindqvist Y (1998) Crystal structure of β-ketoacyl-acyl carrier protein synthase II from *E. coli* reveals the molecular architecture of condensing enzymes. EMBO J 17:1183–1191
26. Davies C, Heath R, White S, Rock C (2000) The 1.8 Å crystal structure and active-site architecture of β-ketoacyl-acyl carrier protein synthase III (FabH) from *E. coli*. Structure 8:185–195
27. Zhu L, Maruvada R, Sapirstein E, Malik KU, Golden M, Kum KS (2010) Arachidonic acid metabolism regulates *E. coli* penetration of the blood–brain barrier. Infect Immun 78:4302–4310
28. Elomaa E (1979) Enterotoxins of *Escherichia coli* and epilepsy. Med Hypotheses 5:707–710
29. Yurtta L, Özkay Y, Gencer HK (2015) Synthesis of new thiazole derivatives and their biological activity evaluation. J Chem 7:1–7
30. Balouiri M, Saddiqui M, Ibnsouda K (2016) Methods for in vitro evaluating antimicrobial activity; a review. J Pharm Anal 6:71–79
31. Sashidhara KV, Rao KB, Kushwara P, Modukuru RK, Singh P, Shukla PK, Chopra S, Pasupeleti M (2015) Novel chalcone-thiazole-hybrids as potent inhibitors of drug resistance *Staphylococcus aureus*. Med Chem Lett 6:809–813
32. Rigaku (2011) CrystalClear SM expert. Rigaku Corporation, Tokyo
33. Sheldrick GM (2008) A short history of SHLX. Acta Crystallogr A A64:112–122
34. Sheldrick GM (2015) SHLXT-integrated space-group and crystal structure determination. Acta Crystallogr C C71:3–8
35. Macrae C, Bruno I, Chisholm J, Edgington P, McCabe P, Pidcock E, Rodriguez L, Taylor R, Streek J, Wood P (2008) New features for visualization and investigation of crystal structures. J Appl Cryst 41:466–470